NASA TECHNICAL MEMORANDUM

NASA TM X-74025

NASA TM X-74025

SHOCK TUBE MEASUREMENTS OF THE OPTICAL ABSORPTION OF TRIATOMIC CARBON, C_3

Jim J. Jones

June 1977

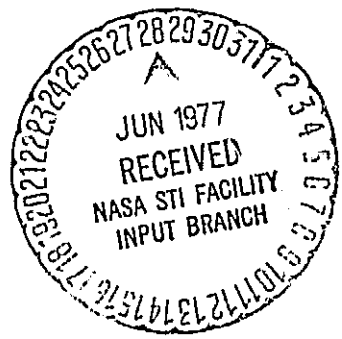

National Aeronautics and Space Administration

Langley Research Center
Hampton, Virginia 23665

1. Report No.	2. Government Accession No.	3. Recipient's Catalog No.
NASA TM X-74025		

4. Title and Subtitle	5. Report Date
Shock Tube Measurements of the Optical Absorption of Triatomic Carbon, C_3	June 1977
	6. Performing Organization Code: 6430
7. Author(s): Jim J. Jones	8. Performing Organization Report No.
	10. Work Unit No.: 506-26-20-01
9. Performing Organization Name and Address: NASA Langley Research Center, Hampton, VA 23665	11. Contract or Grant No.
	13. Type of Report and Period Covered: Technical Memorandum
12. Sponsoring Agency Name and Address: National Aeronautics and Space Administration, Washington, DC 20546	14. Sponsoring Agency Code

15. Supplementary Notes

Early data release - material will be included in conference paper and/or NASA technical note.

16. Abstract

The spectral absorption of C_3 has been measured in a shock tube using a test gas mixture of acetylene diluted with argon. The absorption of a pulsed xenon light source was measured by means of eight photomultiplier channels to a spectrograph and an accompanying drum camera. The postshock test gas temperature and pressure were varied over the range 3300-4300 K and 0.36 to 2.13 atmospheres, respectively.

The results showed appreciable absorption from C_3 for the wavelength range 300 to 540 nanometers. The computed electronic oscillator strength varied from 0.12 to 0.06 as a function of temperature. Uncertainties in the thermodynamic functions for C_3, which are needed to compute number density, are believed to be the principal problem in determining the true value of the oscillator strength.

17. Key Words (Suggested by Author(s))	18. Distribution Statement
Absorption cross section Ablator gas Carbon vapor	Unclassified - Unlimited.

19. Security Classif. (of this report)	20. Security Classif. (of this page)	21. No. of Pages	22. Price*
Unclassified	Unclassified	40	$4.00

* For sale by the National Technical Information Service, Springfield, Virginia 22161

SHOCK TUBE MEASUREMENTS OF THE OPTICAL ABSORPTION OF TRIATOMIC CARBON, C_3

Jim J. Jones

SUMMARY

The spectral absorption of C_3 has been measured in a shock tube using a test gas mixture of acetylene diluted with argon. The absorption of a pulsed xenon light source was measured by means of eight photomultiplier channels to a spectrograph and an accompanying drum camera. The postshock test gas temperature and pressure were varied over the range 3300-4300 K and 0.36 to 2.13 atmospheres, respectively.

The results showed appreciable absorption from C_3 for the wavelength range 300 to 540 nanometers. The computed electronic oscillator strength varied from 0.12 to 0.06 as a function of temperature. Uncertainties in the thermodynamic functions for C_3, which are needed to compute number density, are believed to be the principal problem in determining the true value of the oscillator strength.

INTRODUCTION

Entry into the atmospheres of the outer planets is accompanied by large radiative heating of the probe forebody. To some degree, this thermal radiation is blocked (absorbed) by the cooler gases being evolved from the ablative heat shield. For example, reference 1 shows that the ablation gases emitted from a phenolic carbon heat shield absorb about half the incident radiant energy for an entry into the atmosphere of the planet Jupiter. Although the calculation method used in reference 1 is the best available estimate of the absorption effects of the ablator gases, its accuracy is hampered by the limited knowledge of the absorption properties of the various gas species present. Under the assumption of thermochemical equilibrium, the calculations predict that a significant fraction of the ablator gas will be composed of such molecules as C_3, C_4, C_5, C_2H, and C_3H, for which little or no information is available as to spectral absorption properties.

The present study examines the absorption of triatomic carbon C_3 in the spectral range 260 to 560 nanometers. Reference 1 indicates that C_3 is the dominant species near the ablator wall, with a mole fraction exceeding 0.5 for some cases. Thus, an accurate determination of its spectral absorption cross section will greatly benefit the radiant transfer calculations.

The most prominent spectral feature of C_3 is a continuum-band system in the vicinity of 400 nanometers. Frequently referred to as the 4050 Å Bands (ref. 2), and first observed in cometary spectra, this line group has been shown (ref. 3) to be due to a ground-state connected electronic transition in the C_3 molecule. Only a few lines are observed at cryogenic temperatures (e.g., refs. 4-7), but at elevated temperature, a strong apparent continuum dominates this spectral region (ref. 2). This apparent continuum was shown by Brewer and Engelke (ref. 8) to be due to the same bound states as the observed lines and, therefore, not a true continuum but a "pseudocontinuum" of very closely spaced rotational lines of the electronic transition. Reference 8 includes an absorption measurement in saturated carbon vapor at a temperature of 3200 K. In reference 9, these data were converted to spectral cross section using the estimate of C_3 number density given in reference 8. This appears to be the only quantitative data on C_3 absorption at high temperature that is available in the open literature.

In the present study, the species C_3 was produced by shock heating a C_2H_2 - argon test gas mixture in a shock tube. The calculated temperature behind the incident shock wave, based on shock velocity measurements, ranged from about 3300 to 4300 K. The postshock pressure varied from 0.36 to 2.13 atmospheres. The postshock test gas was viewed in absorption using a high-pressure xenon pulsed light source. The number density was calculated using the measured shock velocity and assuming thermochemical equilibrium. From the measured absorption and calculated number density, the spectral absorption cross section was calculated for the spectral range 260 to 560 nanometers. The present paper presents the basic data, while analysis of the significance of the data will be left to subsequent publications.

SYMBOLS

a_0, a_1, a_2, a_3	coefficients in curve fit of absorption cross section versus temperature (eq. (8))
c	velocity of light
D	film density
E	film exposure
e	charge of an electron
e(t)	time-dependent emission of the test gas as measured by a spectrograph channel photomultiplier tube
F(t)	time-dependent absorption defined by equation (1)
F'(t)	absorption parameter corrected for gas emission, as defined by equation (2)
f_e	electronic oscillator strength
I_0	unattenuated light intensity
I_s	light intensity after passing through test gas with path length s
K_λ, K_ω	extinction coefficient at wavelength λ or wave number ω
m	mass of electron
N	number density
p	pressure
S(t)	time-dependent photomultiplier signal
s	optical path length through test gas
T	temperature
T_2	test gas temperature behind incident shock wave
t	time
V_s	incident shock wave velocity
X	distance along shock tube measured from diaphragm

γ	slope of linear portion of film sensitivity curve (eq. (3))
ΔHf°_{298}	heat of formation at one atmosphere pressure and 298 K
λ	wavelength
ω	wave number

Subscripts:

0	prerun condition for light signal
1	condition before shock arrival
2	condition behind incident shock

EXPERIMENTAL APPARATUS

Shock Tube

The shock tube used in the present investigation is the same facility described in reference 10. It is an all stainless steel tube 15.2 cm in internal diameter with a driven tube approximately 15.4 meters long. The electric arc electrode assembly was removed from the driver chamber and a driver extension section was added to make a driver chamber length of 2.44 meters. The boundary layer splitter plate assembly in the test section was not used, since in the present study, the postshock flow Mach numbers were less than 2 and preliminary tests indicated the splitter plate assembly sometimes choked the flow. Thus, the test section windows were mounted flush with the tube walls.

Helium was used as the driver gas for all runs. After preliminary evacuation, helium was injected into the driver chamber until the diaphragm ruptured. Diaphragms were stainless steel with the conventional grooves machined in a cross pattern to cause the diaphragm to open in the usual four-petal configuration.

The driven chamber was initially evacuated to a pressure of approximately 0.03 N/m^2 using a diffusion pump and liquid-nitrogen cooled trap. The test gas was injected into the chamber approximately 3 to 5 minutes prior to the run. The increase in chamber pressure due to outgassing and leakage was approximately 0.07 N/m^2 per minute. Since the initial test gas pressure was 700 N/m^2 or greater, the ratio of air and water vapor to test gas was believed to be 6×10^{-4} or less for all runs.

Optical Instrumentation

A schematic drawing of the optical arrangement and shock tube is shown in figure 1. The light source was a high pressure xenon lamp which was pulsed by the discharge of a capacitor-inductor transmission line to produce a nearly constant light intensity for about 1 millisecond. This pulse was initiated by the passage of the shock wave at a station upstream of the test section, so that the light pulse was initiated 200 to 300 microseconds prior to the arrival of the shock wave at the window location. Quartz lenses were used to form an image of the lamp on a small orifice 1.8 mm in diameter and then to form a collimated beam using the image at the orifice as the apparent source. Another lens focused this beam on the spectrograph entrance slit. Field stops 1 cm in diameter were used at the window locations and along the collimated beam path to reduce stray light and define the geometry of the optical path.

The spectrograph used was a Czerny-Turner mount with a nominal aperture of f/6.3. Internal masks were used to insure the spectrograph was filled with light. These masks limited the spectrograph to approximately f/8. The spectrograph was modified by inserting a front-surface mirror into the beam from the camera mirror to the focal plane. This mirror reflected approximately 80 percent of the light into a rotating-mirror camera which had been adapted to the spectrograph. The remaining 20 percent of the light passed over the top of the mirror and fell on the focal plane. A group of eight light pipes was mounted with their entrance faces at the focal plane. Each light pipe led to a photomultiplier tube. When used in the ultraviolet, the entrance faces of the light pipes were coated with sodium salicyclate. The effective width of the light pipes ranged from 1.1 to 1.9 mm. Therefore, the effective band pass was 4.3 to 7.7 nanometers and 2.1 to 3.8 nanometers for the two gratings used in the investigations. The gratings used were a 300 line/mm grating blazed at 500 nanometers and a 600 line/mm grating blazed at 300 nm. The approximate values of linear dispersion at the focal plane were 41.0 and 20.2 nanometers/cm, respectively.

The photomultipliers were used with load resistors that limited output current to less than 1 milliamp. The linearity of each photomultiplier tube was checked using neutral density filters. An example of the linearity check is shown on figure 2 for one channel. On each channel, ballast capacitors paralleled each of the last two resistors of the dynode chain so as to maintain nearly constant dynode voltages for extended signal periods.

The drum camera was a commercially manufactured device which was modified to adapt to the spectrograph. It used an air driven turbine to turn the drum 318 ± 5 revolutions/sec. The length of film (internal circumference of the drum) was 31.88 cm and, therefore, the film speed was 10.1 ± 0.1 cm/millisecond. Since the effective slit height at the film was approximately 1.5 millimeters, the time resolution on the film was no better than 15 microseconds.

Velocity-Pressure Instrumentation

The distances from the primary diaphragm to the centers of the instrumentation ports are shown in table I. A thin-film resistance thermometer was installed in station 1 to detect the passage of the shock wave. The output signal from this gage was used to initiate both the system of time-interval meters which measured the shock transit times and the time-delay generators which triggered the oscilloscopes.

The remaining instrumentation ports had either thin-film gages, light pipes leading to photomultipliers, or quartz pressure transducers mounted as indicated in table I. The thin-film gages were used because they gave low-noise, rapid-rising signals which were easily amplified for use as trigger signals. The photomultipliers merely gave a qualitative indication of the approximate test time. The pressure transducers showed the steadiness of the test gas slug. Examples of the oscillograms from a photomultiplier and a pressure transducer are shown in figure 3.

The shock velocity was determined from the measurements of time-interval meters. The amplified signal from the instrumentation mounted at each station was used to stop a time-interval meter. The start gate for all the time interval meters was provided by the station 1 thin-film gage. An example of the calculated average velocity between successive stations is shown in figure 4. The shock attenuation was typically about 18 m/sec/m. The velocity which was used to reduce the data was the average velocity from station 7 to station 12. This interval was selected to be indicative of the average speed of the shock which processed the test gas, and a sufficiently long time period to minimize the error in measuring the transit time of the shock wave.

Test Gas

The test gas was purchased already mixed, and certified by the supplier to be 2.99-percent C_2H_2, 97.01-percent argon by volume. Twice during the test program, a sample of the test gas was analyzed by gas chromatograph to insure the mixture remained uniform. A few runs were made as a check using a 1.97-percent C_2H_2, 98.03-percent argon mixture.

Test Procedure

As mentioned previously, the driven chamber was evacuated to about 0.03 N/m^2 prior to each run. The driver chamber was evacuated to about 1.5 N/m^2 using a mechanical pump only. It was found that if the lamp had not been fired for several hours, it was necessary to fire it several times in order to insure reproducible light pulses. When the lamp had been fired sufficiently to insure good repeatability, a prerun shot was recorded from the eight photomultipliers connected to the spectrograph light pipes. These records were regarded as the unabsorbed intensity as a function of time for each channel. The capacitor bank which fired the lamp was charged to 355 volts, as read on a digital voltmeter, for the prerun record.

After injecting the test gas into the driven tube, the lamp supply capacitors were charged to approximately 365 volts. Since the charge slowly leaked off the capacitors, the succeeding run operation steps were paced in an attempt to synchronize the diaphragm rupture with a capacitor voltmeter reading of 355 volts. This result was accomplished within ±2 volts for nearly all runs.

Following each run, the windows were cleaned since postrun lamp firings showed the intensity was reduced by 10 percent or so due to deposits on the windows. The entire shock tube interior was cleaned periodically (approximately every 20 runs) using trichloroethane as a solvent.

DATA REDUCTION PROCEDURES

Spectrograph Channels

A sample record from a spectrograph channel is shown in figure 5. Figure 5(a) shows the prerun record of the light pulse and figure 5(b) shows the oscillogram taken during the run. The arrival of the shock wave is clearly indicated by the sudden drop in photomultiplier signal level. Figure 5(c) shows the record after being digitized, along with the prerun record for the same channel. Figure 5(d) presents the fraction of light absorbed

$$F(t) = \frac{S_0(t) - S(t)}{S_0(t)} \tag{1}$$

where $S(t)$ and $S_0(t)$ are the time-varying values of the photomultiplier signal for the run and prerun, respectively. For these traces, time equal to zero corresponds to the start of the light pulse.

The parameter $F(t)$ was plotted for each channel of each run using a programable calculator with the digitized oscillograms as input data. Typically, the value of $F(t)$ increased moderately with time after shock passage, most likely because of the growing wall boundary layer. Many runs showed the parameter $F(t)$ took 40 microseconds or so to reach a plateau value, suggesting the chemical relaxation rate took approximately this long to adjust to the postshock condition. The value of the parameter $F(t)$ was read after it first reached a plateau and this value was used in determining the absorption coefficient for the present data.

The light received into the spectrograph included the emission from the gas as well as the (partially absorbed) emission from the lamp. In order to determine the contribution from gas emission, runs were made with the lamp turned off. For some runs, a light chopper was employed so that the absorption and emission could be determined on the same run. The field stops in the light path attempted to insure that the volume of gas contributing to the emission was essentially the same as that for which the absorption was determined.

The emitted light was expressed as a fraction of the prerun lamp signal S_0 and this quantity was used to correct the absorption parameter $F(t)$. Denoting the corrected absorption as $F'(t)$ and the emission as $e(t)$

$$F'(t) = \frac{S_0 t - (S(t) - e(t))}{S_0(t)} = F(t) + \frac{e(t)}{S_0(t)} \qquad (2)$$

For most run conditions, the emission term was immeasurably small. For the highest temperature runs, the emission term grew as large as $\frac{e(t)}{S_0(t)} = 0.1$ and represented a correction to the value of $F(t)$ of the order of 30 percent. A few runs were made in pure argon test gas to insure that the emission and absorption from the carrier were negligible.

Drum Camera Film

A sample of the film obtained from the drum camera is shown in figure 6(a). The prominent features of the absorption are an apparent continuum and a few bands. All the bands that were observed over the entire wavelength range of the study belong either to C_2 or the Violet System of CN. This latter system is so strong that only a small contamination of air in the test gas mixture causes it to appear.

Figure 6(b) shows a microdensitometer tracing of the film for the same run as that of figure 6(a). Two traces are shown, one taken at a time just before shock arrival and the other taken about 100 microseconds after shock arrival. The difference between the traces is a measure of the absorption.

The film yields so much more spectral detail than the light pipe channels that an attempt was made to use the densitometer traces quantitatively. The following procedure discusses how this was done. It must be emphasized, however, that very little confidence can be attached to the quantitative film density results, because of the many pitfalls associated with using film quantitatively, and the approximate procedure used in the present study.

Twice during the investigation, sensitometer samples were made on film samples and these were developed in the same manner as the test films. The sensitometer samples were then run on the microdensitometer and a plot of the films' specular density versus the logarithm of the exposure was constructed as shown in figure 7. The linear portion of this curve showed a slope of approximately $\gamma = 0.9$. The film density D was thus assumed to be related to exposure by

$$D_1 - D_2 = \gamma[\log_{10}(E_1) - \log_{10}(E_2)] \qquad (3)$$

where the subscripts 1 and 2 indicate times just before and just after shock arrival, respectively. Since exposure is defined as the product of the light intensity and time, equation (3) may be rewritten

$$\frac{E_1}{E_2} = \frac{I_1 t}{I_2 t} = 10^{(D_1 - D_2)/\gamma} \tag{4}$$

Since the exposure time is the same for each element on the test film, equation (4) yields the ratio of light intensity before shock arrival to that after the shock as a function of density difference on film. This ratio was then used to determine the wavelength dependent extinction coefficient, K_λ. As noted previously, the values of extinction coefficient determined from the film must be viewed with great caution. However, as will be shown subsequently, they show quite good repeatability and are in essential agreement with the data obtained from the light pipe-photomultiplier channels. The two most daring assumptions in the procedure just described appear to be:

1. The determination of the slope γ was made using the sensitometer's xenon flash lamp and this "white" light data was then assumed to apply for all wavelengths throughout the spectral range of the investigation, and for all film exposures, even though at low film density, the slope was distinctly lower.

2. The same calibration data were assumed to apply for all runs, thus ignoring any differences in film development from run to run.

Absorption Cross Section

The extinction coefficient is defined by the relation

$$dI = -K_\lambda(s) I ds \tag{5}$$

(see ref. 11 for a review of fundamentals in absorbing media). If the absorbing medium has uniform absorbing and scattering properties along the length of the light path s, equation (5) may be integrated from o to s to yield

$$K_\lambda = \left(\ln \frac{I_o}{I_s}\right)/s \tag{6}$$

Here, I_o and I_s denote, respectively, the intensity as the light beam enters and leaves the absorbing medium of length, s.

In the present study, scattering effects were ignored and the absorption coefficient was assumed identical to the extinction coefficient. Solid state particles, if present, would be expected to be a significant scattering agent. For this reason, the present test conditions avoid the lower temperature range where solid carbon particles might be expected to be present.

The data are presented as an absorption cross section

$$\sigma_\lambda = \frac{K\lambda}{N_{C_3}} \tag{7}$$

The number density N_{C_3} was obtained by means of the Aerotherm Chemical Equilibrium (ACE) computer program of reference 12. For the data presented in the tables, the density is based on a heat of formation of C_3, ΔHF°_{298} = 196 kilocalories per mode. This value is not very firmly established, although a number of investigators have addressed the subject. Reference 13 reviews the various attempts up to 1969 to determine the heat of formation of C_3. In presenting the present data, sufficient information is given in the tables to permit the recalculation of C_3 number density using a different value of the heat of formation.

Using the value ΔHf°_{298} = 196 kilocalories per mole, the ACE program predicts that C_3 will be one of the most abundant species present in the postshock flow. Figure 8 shows the mole fractions of the principal species which are predicted to be present behind a shock wave as a function of the shock velocity. For this example, the initial pressure was held constant at 1.72 kN/m^2, which is typical for the present data. Argon, which of course is the most abundant species, has been omitted from figure 8, but the others are shown to be H, H_2, C, C_2, C_3, C_2H, and C_3H. Of these, the first four have well identified spectra which may be recognized and subtracted out if they appear in the present data. The spectra of the latter two, C_2H and C_3H are not known, however, so any contribution they may make to the present absorption data may go unrecognized. C_3H has a distinctly different variation of abundance with temperature than C_3, so examination of the absorption profile at different temperatures would help answer the question of whether or not C_3H contributed to the absorption in this spectral range. The similarity of the temperature variation of C_2H and C_3 may not permit this technique to be used. Main and Bauer have synthesized an electronic spectrum for C_2H in reference 14. Of the eight electronic transitions given in reference 14, none fall in the present spectral range.

RESULTS AND DISCUSSION

The basic experimental results are presented in table II for the 3-percent mixture and table III for the 2-percent mixture. The shock velocity and postshock temperature and pressure are tabulated as well as the absorption cross sections obtained from the eight spectrograph channels. For each channel, the central wavelength for each light pipe is noted, and the corresponding cross-section measurement is given directly below. For certain wavelength settings of the grating, some "stray light" was noted on channels 1 and 2. Where this occurred, data from these channels are not included. Here the term stray light refers to light emanating from the pulsed light source, but of the wrong wavelength for that particular channel.

At each grating position, a check for stray light was made by means of a series of band-pass filters inserted in the light beam at the entrance slit to the spectrograph.

Constant Temperature Survey

Figure 9 presents the absorption cross section for seven runs in which the postshock test state was repeated as closely as possible. The temperature was 3694 ± 28 K for these runs, which are runs 1-7 in table II. Between these runs, the grating position was changed to move the spectral setting of the channels by about 35 nanometers. Thus, a complete spectral survey was obtained at nearly constant test conditions. Figure 9 shows the photomultiplier data for the seven runs by circular symbols. For three of these runs, the data from the densitometer readings of the film are shown as solid lines. Also shown, as a dashed curve, are the data of reference 8; this latter curve has been reduced by a factor of four to facilitate comparison.

Figure 9 shows that the general character of the absorption profile for the present data at a temperature of 3700 K is very similar to that obtained by Brewer and Engelke (ref. 8); but their data, obtained at 3200 K, is more than four times greater in amplitude. The absorption profile shows no distinctive features except those due to the Violet Band system of CN and the Swan band system of C_2. It might be noted that these bands were observed also by Brewer and Engelke, but were "faired out" (see fig. 1 of ref. 8).

No data were presented in reference 8 for wavelengths shorter than 370 nanometers. For less than 370 nm, the present data show a continuation of the downward trend to about 300 nm, at which point the cross section becomes nearly constant. The data for this shortest wavelength region (below 300 nm) must be viewed with some skepticism. The light output of the xenon flash lamp was very low in this region, resulting in poor signal-to-noise ratio on the photomultiplier channels and susceptibility to stray light contamination. Also, insufficient data were obtained at these wavelengths to indicate whether the absorption was due to C_3 or some other species.

Temperature Variation of Absorption Cross Section

For each setting of the spectrograph grating, a number of runs were made with varying shock strengths and, thus, the temperature effect on absorption was determined at a number of wavelengths. A total of 26 different wavelengths was available with which to determine the temperature effect on absorption cross section. In figure 10, eight of these wavelengths are presented and the experimentally determined absorption cross section is shown over the temperature range of the experiment. Also shown for each wavelength is a least-squares curve fit to the data of the form

$$\sigma_\lambda = a_0 + a_1 T + a_2 T^2 + a_3 T^3. \qquad (8)$$

The curve fit equations may then be used to generate an approximate spectral absorption profile for any specified temperature within the temperature range of the experiment. In figure 11, such profiles are shown for four selected temperatures. In figure 11, the value of equation (8) is shown at each wavelength with a symbol. The vertical bar shows the standard deviation of the data from the curve for that wavelength setting. Absence of a bar indicates insufficient data to determine standard deviation.

The spectral absorption curve fits shown in figure 11 indicate that for the temperature range 3400 to 4000 K, the profiles remain quite similar. However, there appears to be some change with temperature in the general amplitude. The amplitude is highest at the low temperature extreme (3400 K) and decreases to a minimum at about 3800 K. Figure 10 showed that at most wavelengths, this trend is displayed with the minimum usually occurring near 3800 K. At temperatures of 4000 K and above, the general trend is for the absorption cross section to rise, but the very limited data in this temperature range do not permit a firm conclusion.

The fact that the wavelength-integrated cross section (i.e., the area under the curve in fig. 11) does not appear to remain constant with temperature is a matter of some concern with regard to the consistency of the data. It can be shown (e.g., ref. 15) that for a given transition, the integral of the spectral absorption coefficient is independent of temperature and proportional to the electronic oscillator strength. Thus,

$$\int_0^\infty K_\omega d\omega = \frac{\pi e^2}{mc^2} N f_e \tag{9}$$

in which ω is wave number, f_e is the electronic absorption oscillator strength, and N is the number density of the absorbing state. Since, for the present transition the absorbing state is the ground state, N may be taken as the total number density of C_3. Equation (9) may then be solved for f_e to give

$$f_e = 1.14 \times 10^{12} \int_0^\infty \sigma_\omega d\omega. \tag{10}$$

For the present results, the integral of the absorption cross section was approximated by using the curve fits (eq. (8)) for each wavelength to define σ_ω as a function of temperature and the integral was determined using the trapezoidal rule. For this calculation, certain wavelength channels were believed to be influenced by the C_2 Swan bands, so only 21 channels were included in the computation. The results of this computation are presented in figure 12. The computed oscillator strength is seen to vary from 0.12 to 0.06 over the temperature range 3400 to 4200 K. This may be compared with the value $f_e = 0.13$ quoted for the single measurement in reference 8. For the sake of comparison with reference 8, the value of f_e was computed at $T = 3200$ K and is shown in figure 12, but it should be noted that this temperature is below the range supported by the present

experimental data and is simply an extrapolation of the temperature-dependent curve fits. The result at 3200 K is in good agreement with reference 8, however.

The variation of the computed oscillator strength over the temperature range of the investigation can be caused either by errors in absorption measurement or by errors in computing the number density of C_3. Although other absorbers might possibly be contributing to the absorption results, a more likely cause appears to be equilibrium composition error. Computation of number density is sensitive to the heats of formation and specific heat variations used for the various species present and the uncertainty in these quantities is sufficient to account for the apparent temperature variation of the oscillator strength in the present data.

CONCLUDING REMARKS

The optical absorption of triatomic carbon, C_3, has been measured in a shock tube using a test gas mixture of acetylene diluted with argon. The temperature behind the incident shock ranged from about 3300 to 4300 K and the corresponding pressure varied from 0.36 to 2.13 atmospheres. Appreciable absorption was measured from about 300 nanometers wavelength to about 540 nanometers. Absorption was also noted below 300 nanometers, but the lack of sufficient data and poor signal-to-noise ratio in this wavelength range precluded a firm determination that this short wavelength absorption was due to C_3.

The absorption profile was very similar to that measured by Brewer and Engelke in a furnace. But their measurement, which was taken at a temperature of 3200 K, was about four times greater in terms of absorption cross section than the present measurements at 3700 K. Also, they did not make measurements below 370 nanometers and thus did not include the short wavelength portion of the profile determined in the present study.

Data taken for a narrow passband at specific wavelengths over a range of temperature and pressure reveal a temperature variation of the spectral absorption cross section. Curve fits for these data were obtained for 21 wavelengths, and using these curve fits, approximate spectral profiles can be constructed for any selected temperature within the valid range of the data. If such profiles are integrated with respect to wave number, an electronic oscillator strength is obtained for the transition. This oscillator strength varied from 0.12 to 0.06 over the temperature range 3400 to 4200 K, which may be compared to a value of 0.13 quoted by Brewer and Engelke.

The absorption cross section is determined not only by the absorption coefficient measured, but also by the computed number density of the absorbing state. This latter quantity was computed in the present study using an equilibrium, free-energy minimization computer program which assumed a value of the heat of formation for C_3 of 196 kilocalories per

mole at a temperature of 298 K. Uncertainties in the correct value of the heat of formation of C_3, the correct thermodynamic properties of C_3, and the heats of formation of other hydrocarbon species present in the test gas mixture are a major source of concern in the present data, and are a likely cause of the anomalous variation of the oscillator strength with temperature.

REFERENCES

1. Moss, James N.; Anderson, E. Clay; and Bolz, Charles W., Jr.: Viscous-Shock-Layer Solutions With Radiation and Ablation Injection for Jovian Entry. AIAA Paper 75-671, May 1975.

2. Marr, G. V.; and Nicholls, R. W.: The Emission of the 'λ4050Å' Bands and an Associated Violet Continuum in Oxyacetylene Flames. Canadian J. of Physics, vol. 33, 1955, pp. 394-396.

3. Gausset, L.; Herzberg, G.; Lagerquist, A.; and Rosen B.: Analysis of the 4050Å Group of the C_3 Molecule. Astrophysical J., vol. 142, 1965, pp. 45-76.

4. Weltner, W., Jr.; Walsh, P. N.; and Angell, C. L.: Spectroscopy of Carbon Vapor Condensed in Rare-Gas Matrices at 4° and 20° K. - I. J. of Chemical Physics, vol. 40, no. 5, March 1964, pp. 1299-1305.

5. Weltner, W., Jr.; and McLeod, D., Jr.: Spectroscopy of Carbon Vapor Condensed in Rare-Gas Matrices at 4° and 20° K. - II. J. of Chemical Physics, vol. 40, no. 5, March 1964, pp. 1305-1316.

6. Weltner, W., Jr.; and McLeod, D., Jr.: Spectroscopy of Carbon Vapor Condensed in Rare-Gas Matrices at 4° K. - III. J. of Chemical Physics, vol. 45, no. 8, October 1966, pp. 3096-3105.

7. Barger, R. L.; and Broida, H. P.: Spectra of C_3 in Solidified Gases at 4° and 20° K. J. of Chemical Physics, vol. 43, no. 7, October 1965, pp. 2364-2370.

8. Brewer, L.; and Engelke, J. L.: Spectrum of C_3. J. of Chemical Physics, vol. 36, no. 4, February 1962, pp. 992-998.

9. Jones, Jim J.; Boughner, Robert E.; Haggard, Kenneth V.; Nealy, John E.; Schryer, David R.; and Zoby, Ernest V.: Radiative Property Data for Venusian Entry. A Compendium, NASA SP-348, 1974.

10. Nealy, John E.: Performance and Operating Characteristics of the Arc-Driven Langley 6-Inch Shock Tube. NASA TN D-6922, 1972.

11. Siegel, Robert; and Howell, John R.: Thermal Radiation Heat Transfer. Vol. III - Radiation Transfer With Absorbing, Emitting and Scattering Media. NASA SP-164, 1971.

12. Powers, Charles A.; and Kendall, Robert M.: Users Manual - Aerotherm Chemical Equilibrium (ACE) Computer Program. Aerotherm Corporation, May 1969.

13. Palmer, Howard B.; and Shelef, Mordecai: Vaporization of Carbon in Chemical Physics of Carbon. vol. 4, Marcel Dekker, 1969.

14. Main, Roger P.; and Bauer, Ernest: Equilibrium Opacities of Selected Materials at High Temperatures. Aeronutronic Division of Philco Corporation, Report U-3304, October 1965.

15. Bates, D. R.: Atomic and Molecular Processes. Academic Press, 1962.

TABLE I

SHOCK TUBE INSTRUMENTATION PORT LOCATIONS
AND TYPE OF DETECTOR

Station	Distance From Diaphragm (m)	Detector
1	2.889	H.T.*
2	4.417	P.*
3	5.925	P.
4	7.447	H.T.
5	8.357	P.M.*
6	8.662	P.
7	9.566	P.
8	11.092	P.
9	12.617	H.T.
10	14.126	P.
11	14.940	P.M.
12	15.149	P.
Test Window	15.289	----

*H.T. Thin-Film heat transfer gage.
P. Pressure transducer
P.M. Photomultiplier

TABLE II

TEST CONDITIONS AND MEASURED ABSORPTION CROSS SECTIONS

Test Gas: 2.99-Percent C_2H_2, 97.01-Percent Argon

Run	V_s, m/sec	T_2, K	P_2, kN/m	$N_{C_3} \times 10^{-16}$	λ, nm $\sigma_\lambda \times 10^{18}$, cm^2							
					1	2	3	4	5	6	7	8
1	2259	3686	101	1.45	254 2.71	266 2.47	282 2.47	297 2.39	311 2.71	325 3.33	340 4.15	353 4.63
2	2259	3686	101	1.45	289 2.31	302 2.31	317 3.33	333 3.62	346 4.38	360 5.16	375 7.29	388 5.77
3	2259	3686	101	1.45	325 3.14	337 3.42	352 4.38	368 4.89	381 5.77	395 6.46	410 3.42	423 2.31
4	2278	3723	102	1.48	360 4.40	373 5.18	388 5.63	403 4.40	416 2.48	430 2.11	445 1.16	458 1.10
5	2250	3669	100	1.42	396 5.70	408 3.89	423 2.43	438 1.64	451 1.14	465 2.59	480 0	493 0.59
6	2249	3666	100	1.42	431 2.36	444 1.45	459 1.58	473 0.81	486 0.64	500 1.15	515 3.49	528 0.49
7	2252	3672	100	1.43	466 3.02	479 0.38	494 0.38	508 2.06	521 0.24	535 0.09	550 0.75	563 0
8	2249	3680	113	1.56			397 5.83	426 2.75	454 1.62	482 1.27	512 2.01	537 0.83
9	2185	3551	107	1.31			397 8.31	426 3.27	454 2.08	482 1.43	512 3.57	537 1.43
10	2216	3613	110	1.43			397 8.40	426 3.77	454 1.9	482 1.50	512 3.00	537 1.32

TABLE II - Continued.

Run	V_s m/sec	T_2 K	p_2 kN/m	N_{C_3} $\times 10^{-16}$	λ, nm $\sigma_\lambda \times 10^{18}$, cm^2							
					1	2	3	4	5	6	7	8
11	2051	3322	185	1.05			397 15.0	426 8.0	454 4.95	482 3.70	512 4.9	537 2.7
12	2256	3725	158	2.02			397 7.82	426 3.60	454 1.94	482 1.50	512 2.82	537 1.50
13	2210	3664	215	2.27			397 11.31	426 4.51	454 2.31	482 1.42	512 2.72	537 1.43
14	2557	4177	77	0.54			397 8.9	426 4.33	454 1.83	482 0.62	512 5.23	537 3.18
15	2166	3571	208	1.93			397 13.3	426 6.94	454 3.77	482 3.67	512 3.77	537 3.47
16	2233	3647	112	1.51			405 5.85	434 2.15	461 1.13	490 0.56	520 1.13	545 0.66
17	2238	3657	112	1.53			405 7.12	434 2.89	461 1.72	490 1.06	520 1.72	545 1.47
18	2340	3816	87	1.29			405 6.3	434 2.95	461 1.60	490 0.95	520 2.19	545 1.81
19	2293	3729	83	1.26			405 4.9	434 2.16	461 1.29	490 0.66	520 1.50	545 0.85
20	2547	4128	60	0.43			405 3.70	434 2.50	461 1.95	490 0.94	520 2.47	545 2.47

TABLE II - Continued.

Run	V_s m/sec	T_2 K	p_2 kN/m	$N_{C_3} \times 10^{-16}$	λ, nm $\sigma_\lambda \times 10^{18}$, cm^2							
					1	2	3	4	5	6	7	8
21	2176	3594	210	2.01			405 9.18	434 4.16	461 2.46	490 1.78	520 2.76	545 1.56
22	2334	3847	126	1.78			405 5.96	434 3.09	461 2.13	490 1.52	520 2.87	545 2.08
23	2451	4022	98	1.16			405 3.62	434 2.24	461 2.41	490 1.29	520 3.19	545 2.16
24	2337	3719	37	0.60			405 3.68	434 1.84	461 1.15	490 1.15	520 0.45	545 0.45
25	2164	3446	52	0.75			405 6.95	434 2.54	461 0.45	490 0.74	520 ---	545 0.36
26	2136	3406	61	0.77			405 7.17	434 2.48	461 0.44	490 0.26	520 0.26	545 0.72
27	2626	4289	64	0.24			405 6.78	434 6.35	461 7.63	490 3.56	520 4.19	545 6.78
28	2541	4150	77	.60			405 5.52	434 4.18	461 2.51	490 0.55	520 0.92	545 2.17
29	2459	4036	96	1.11			405 5.41	434 2.97	461 1.98	490 0.62	520 0.96	545 2.07
30	2267	3714	116	1.62			405 5.62	434 2.22	461 1.91	490 0.93	520 0.43	545 0.98

TABLE II - Continued.

Run	V_s m/sec	T_2 K	p_2 kN/m	N_{C_3} × 10^{-16}	λ, nm $\sigma_\lambda \times 10^{18}$, cm^2							
					1	2	3	4	5	6	7	8
31	2258	3736	170	2.14			405 5.09	434 2.10	461 1.07	490 0.32	520 ---	545 0.75
32	2153	3508	153	1.47			405 8.16	434 3.06	461 1.34	490 1.09	520 0.67	545 1.09
33	2086	3399	192	1.29			405 11.7	434 4.42	461 1.93	490 1.00	520 1.24	545 1.71
34	2374	3920	127	1.73	301 3.03	314 2.62	329 3.98	344 3.47	357 4.56	371 4.56	386 6.1	400 5.25
35	2480	4076	100	1.07	301 3.13	314 2.37	329 3.34	344 4.50	357 6.26	371 2.93	386 8.03	400 4.25
36	2474	4063	98	1.07	301 2.64	314 2.65	329 2.19	344 3.34	357 5.18	371 5.03	386 7.38	400 4.63
37	2661	4367	65	0.16	301 4.34	314 6.71	329 7.69	344 9.21	357 15.92	371 9.21	386 23.93	400 11.32
38	2535	4106	59	0.46	301 3.22	314 4.15	329 4.74	344 5.14	357 7.37	371 6.89	386 11.2	400 5.99
39	2372	3875	89	1.27	301 1.99	314 2.47	329 2.64	344 3.09	357 4.73	371 3.58	386 5.73	400 4.73
40	2254	3689	115	1.59	301 2.70	314 2.86	329 3.99	344 4.22	357 5.25	371 5.56	386 7.31	400 5.72

TABLE II - Concluded.

Run	V_s m/sec	T_2 K	p_2 kN/m	N_{C_3} $\times 10^{-16}$	λ, nm $\sigma_\lambda \times 10^{18}$, cm^2							
					1	2	3	4	5	6	7	8
41	2107	3420	148	1.22	301 4.93	314 5.2	329 6.85	344 7.46	357 9.22	371 9.22	386 10.57	400 9.53
42	2174	3463	51	0.76	301 2.85	314 3.74	329 3.74	344 4.88	357 6.37	371 6.93	386 7.96	400 6.94
43	2254	3598	46	0.77	301 2.44	314 2.79	329 3.53	344 3.93	357 4.34	371 4.62	386 6.78	400 4.62
44	2133	3401	61	0.76	301 2.72	314 3.08	329 4.26	344 5.16	357 5.98	371 6.70	386 9.84	400 6.89
45	2239	3660	112	1.53			256 3.33	272 2.94	285 3.39	299 2.55	314 2.55	328 2.94
46	2350	3835	87	1.28			256 2.65	272 3.05	285 2.58	299 2.81	314 2.81	328 2.81
47	2123	3381	60	0.72			256 4.70	272 4.70	285 2.62	299 3.18	314 4.70	328 3.87

TABLE III

TEST CONDITIONS AND MEASURED ABSORPTION CROSS SECTIONS
Test Gas: 1.97-Percent C_2H_2, 97.01-Percent Argon

Run	V_s m/sec	T_2 K	p_2 kN/m^2	N_{C_3} × 10^{-16}	λ, nm $\sigma_\lambda \times 10^{18}$, cm^2							
					1	2	3	4	5	6	7	8
48	2408	4219	78	0.22			405 3.80	434 3.80	461 3.13	490 0.60	520 ---	545 3.8
49	2368	4140	88	0.39			405 6.05	434 1.79	461 2.76	490 ---	520 ---	545 2.76
50	2353	4107	87	0.43			405 4.19	434 2.48	461 1.95	490 ---	520 ---	545 1.61
51	2232	3882	110	1.01			405 4.91	434 2.51	461 1.45	490 ---	520 ---	545 1.61
52	2250	3921	112	0.98			405 4.02	434 2.59	461 2.59	490 0.71	520 0.71	545 1.09
53	2114	3655	146	1.36			405 5.82	434 2.47	461 1.39	490 1.08	520 0.79	545 1.20
54	2156	3749	153	1.46			405 5.41	434 2.30	461 1.60	490 0.57	520 0.47	545 1.00
55	2072	3578	186	1.46			405 7.23	434 2.69	461 1.12	490 0.47	520 0.47	545 0.73
56	2075	3577	165	1.36			405 7.30	434 2.63	461 1.20	490 0.96	520 0.62	545 0.78
57	2195	3823	134	1.28			405 4.59	434 2.18	461 1.48	490 0.65	520 0.43	545 1.27

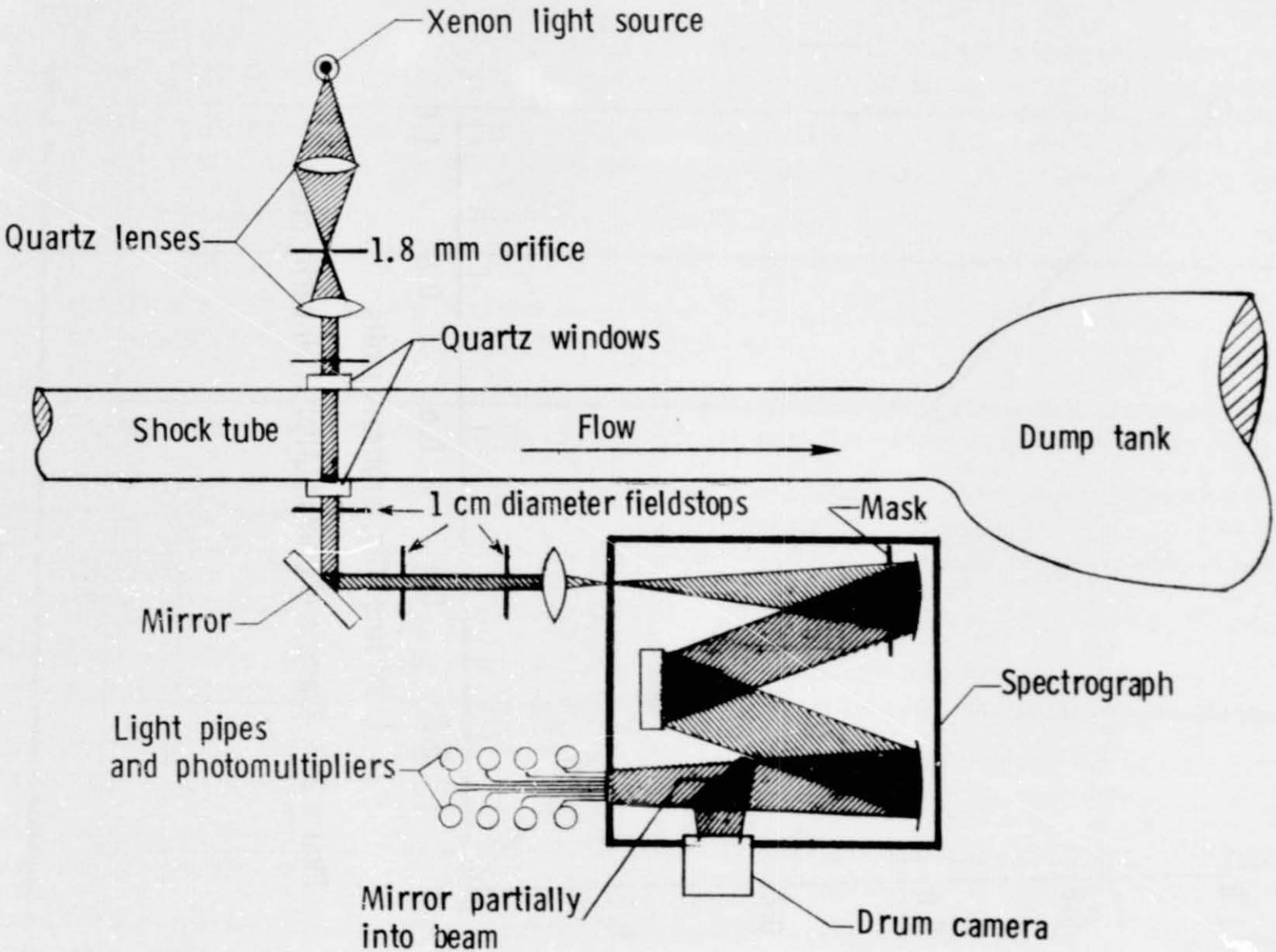

Figure 1.- Schematic of shock tube test location and optical arrangement.

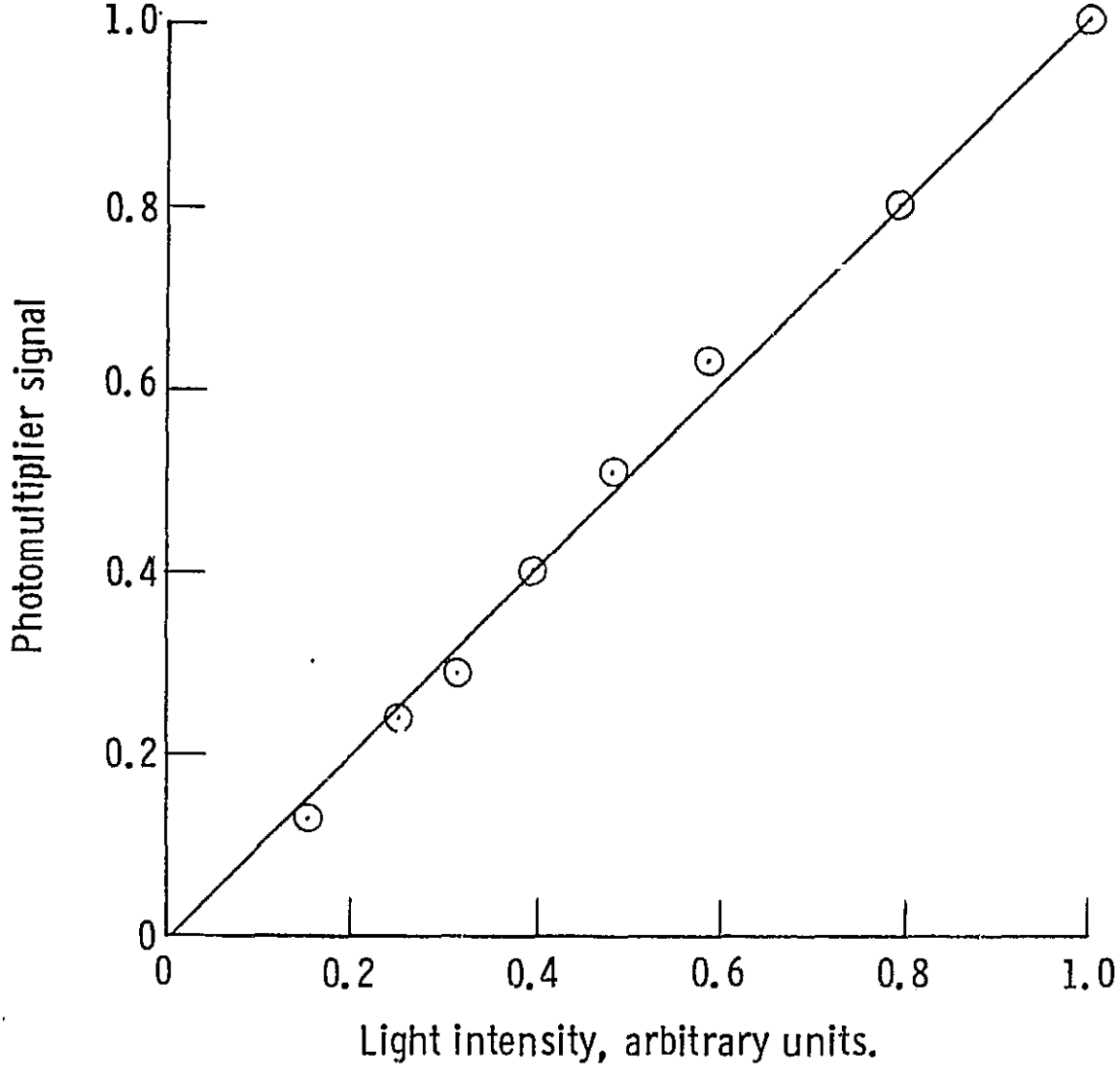

Figure 2. - Exampie of photomultiplier linearity check.

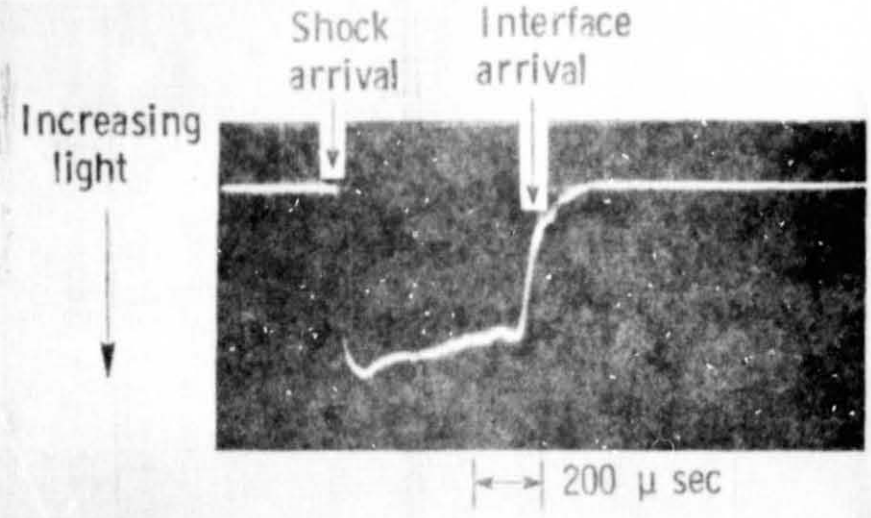

(a) Photomultiplier traces.

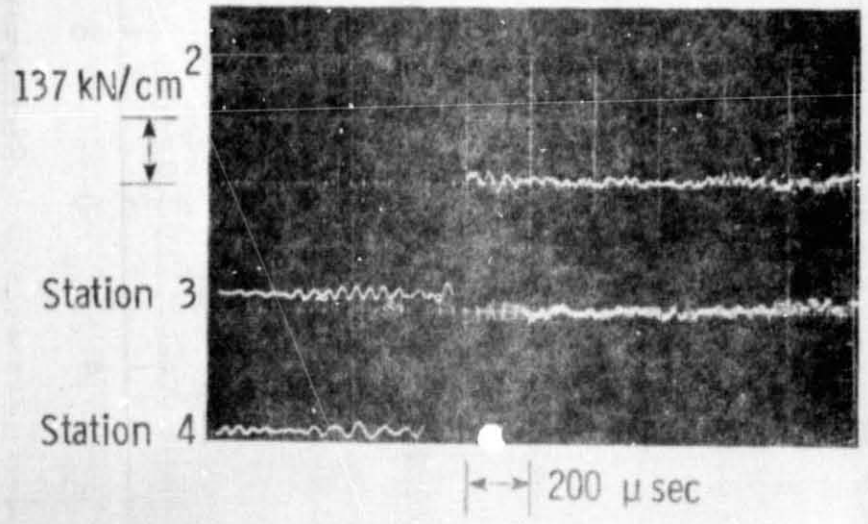

(b) Sample pressure traces. Note: the traces have different start times.

Figure 3. - Sample oscillograms shown photomultiplier and pressure transducers as shock detectors.

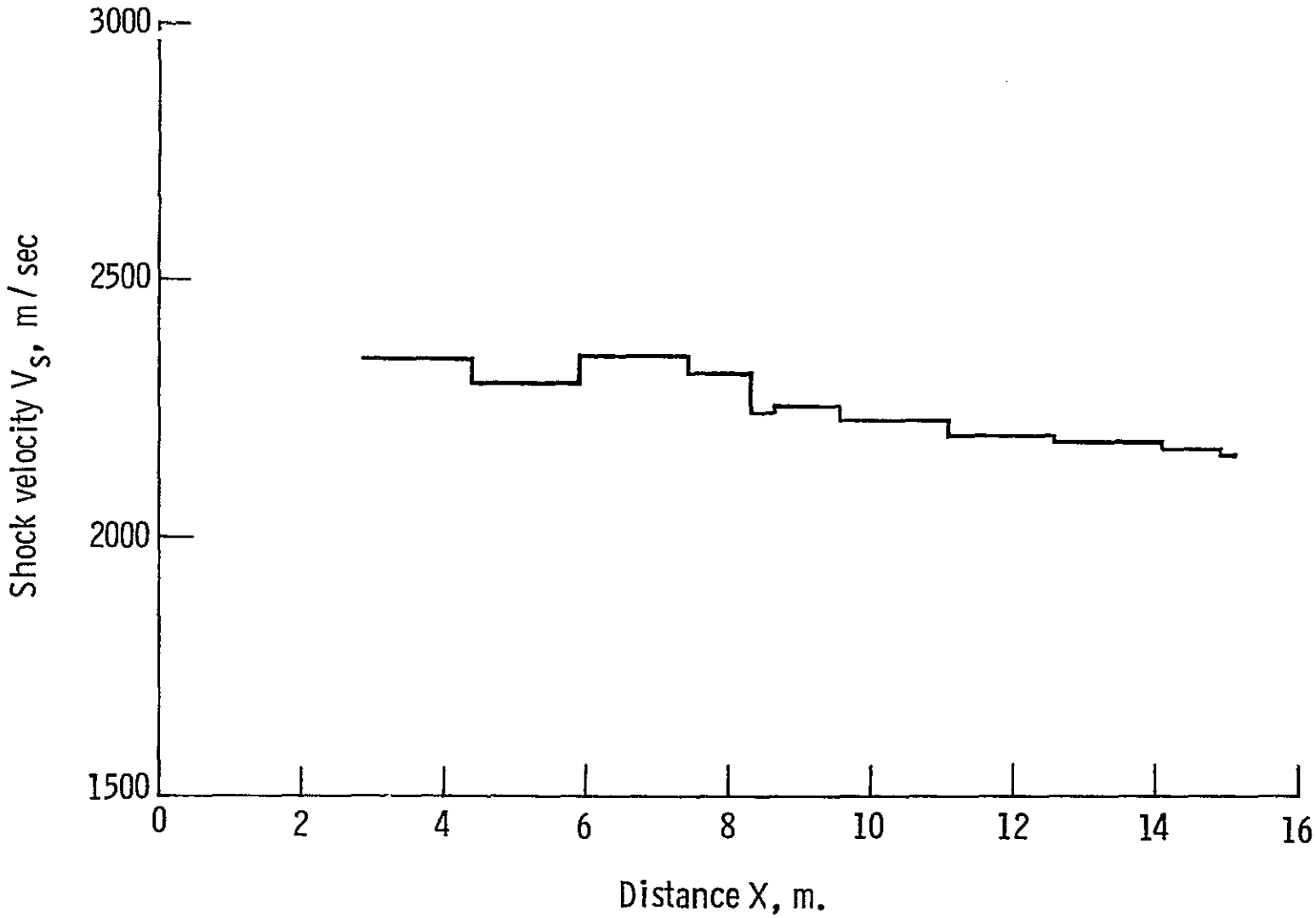

Figure 4. - Shock velocity as determined from time intervals between stations.

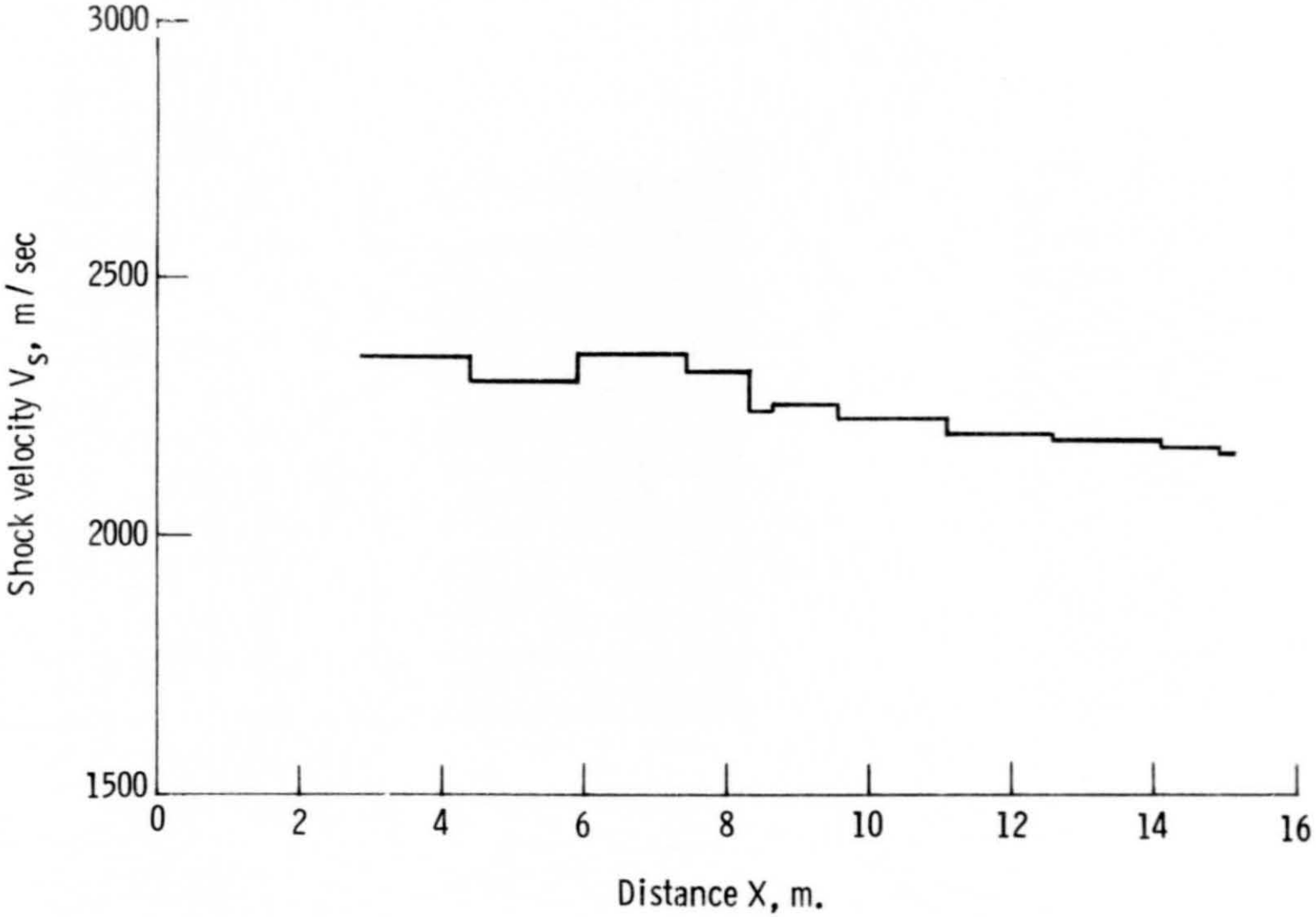

Figure 4. - Shock velocity as determined from time intervals between stations.

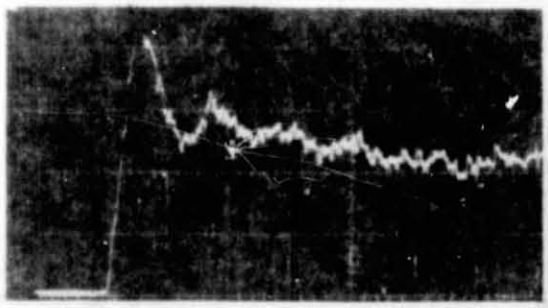

(a) Prerun light pulse.

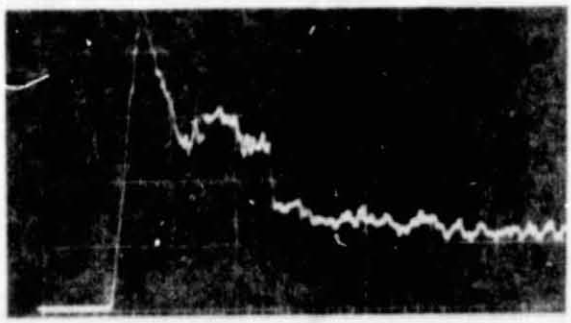

(b) Light pulse during run.

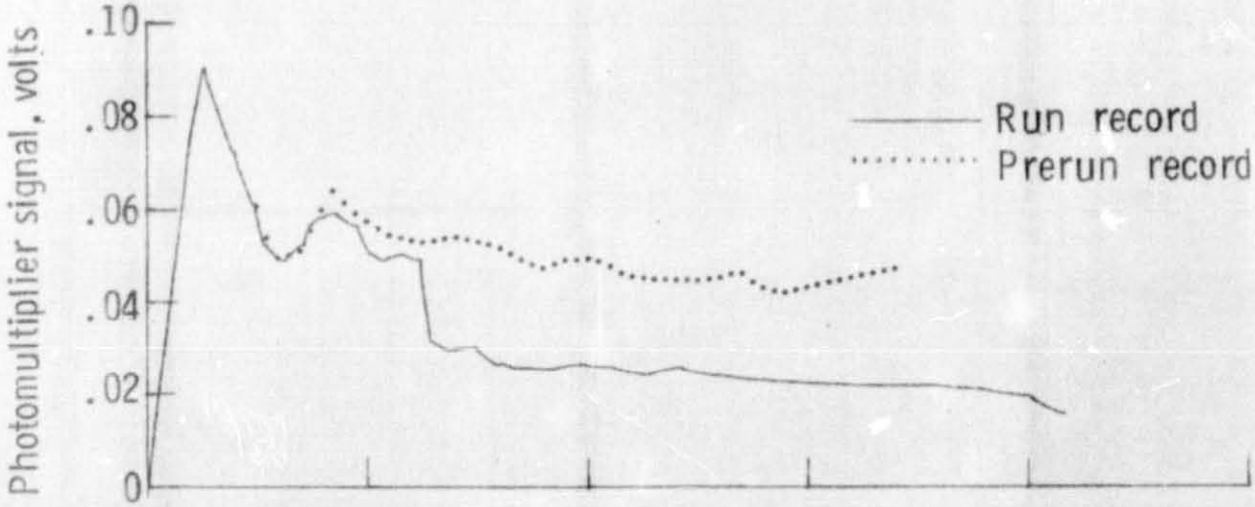

(c) Digitized records of run and prerun traces.

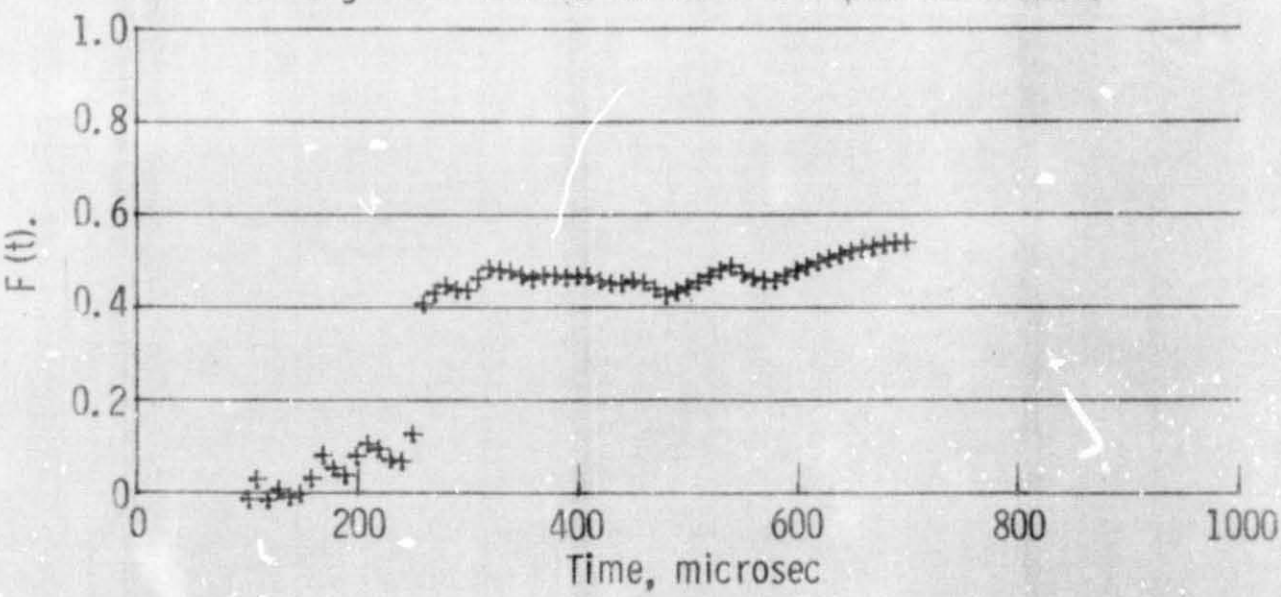

(d) Absorption parameter F(t).

Figure 5. - Sample spectrograph channel record and method of determining absorption parameter F (t).

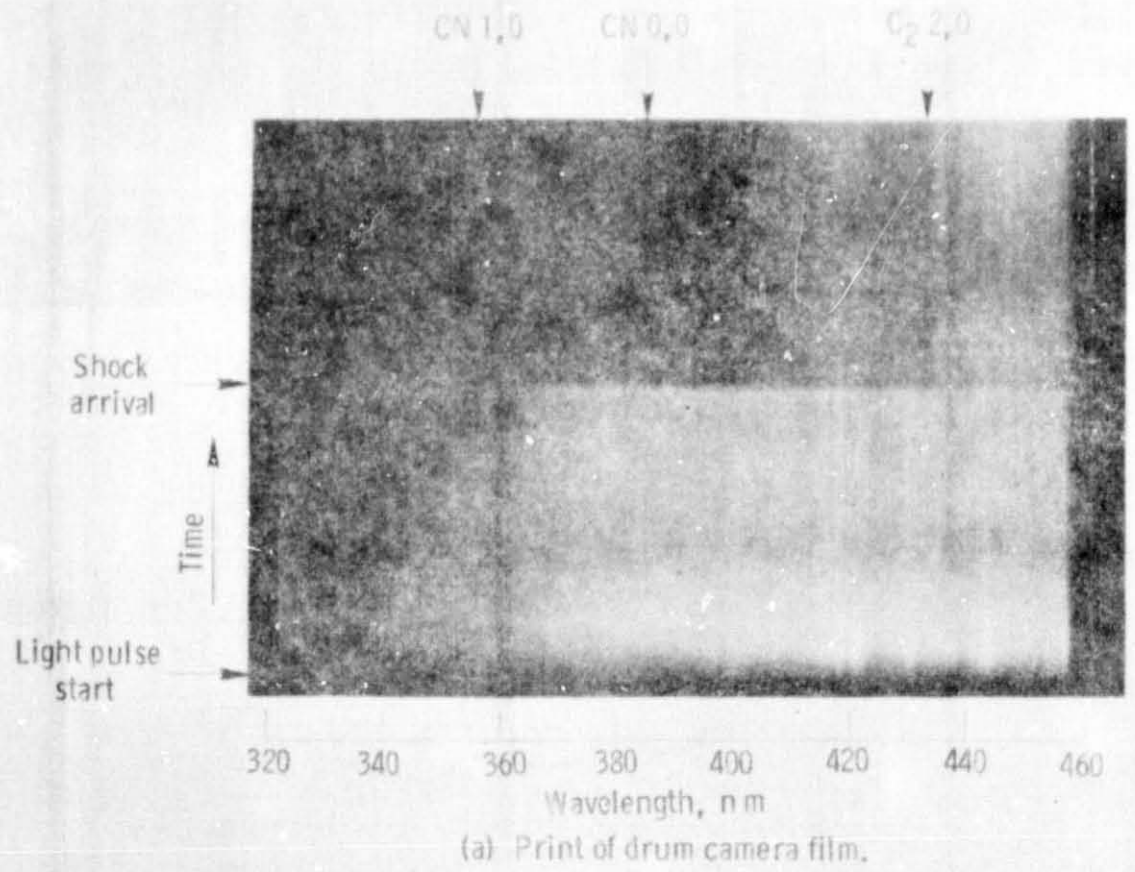

(a) Print of drum camera film.

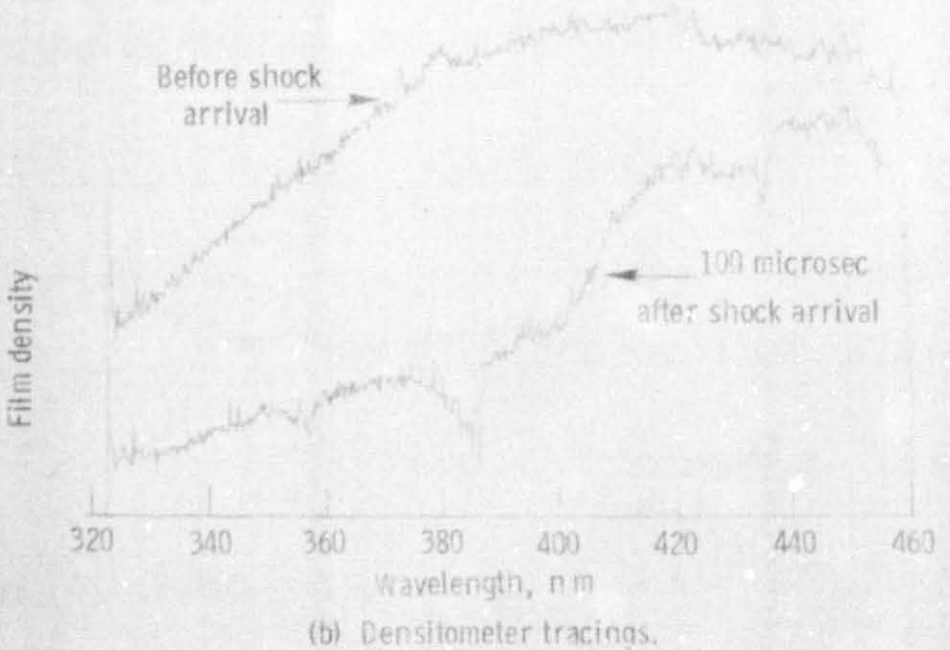

(b) Densitometer tracings.

Figure 6. - Sample drum camera record and densitometer tracings.

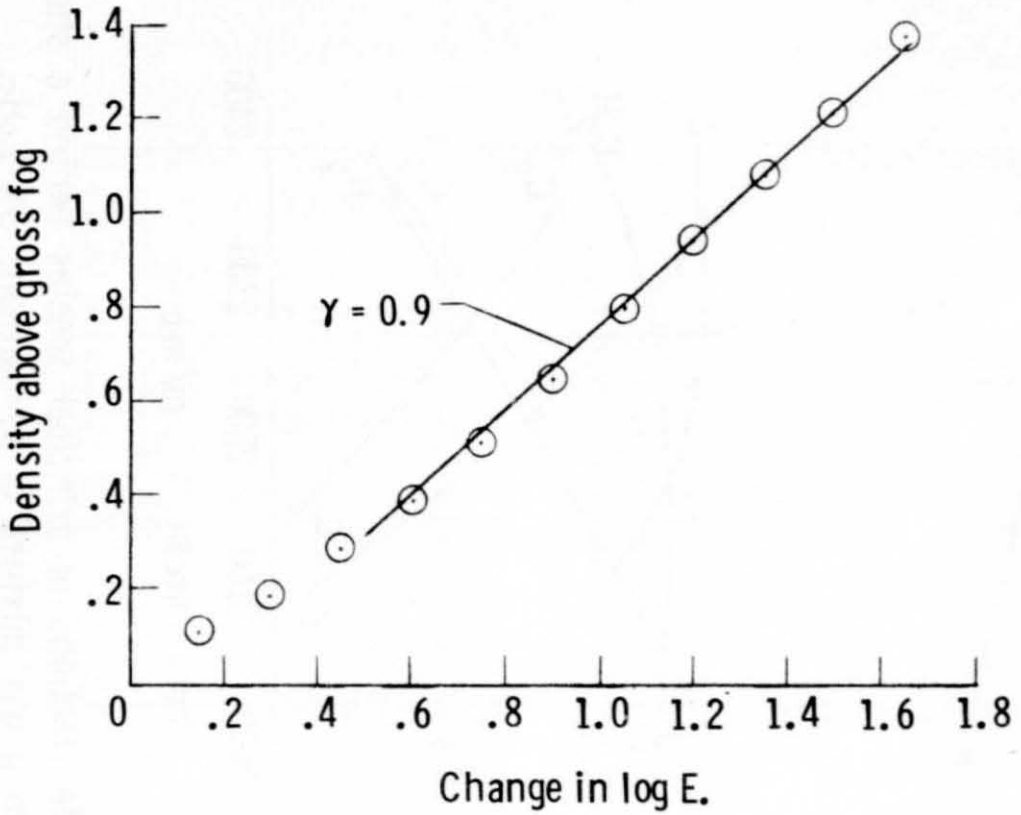

Figure 7. - Results of sensitometer calibration of film.

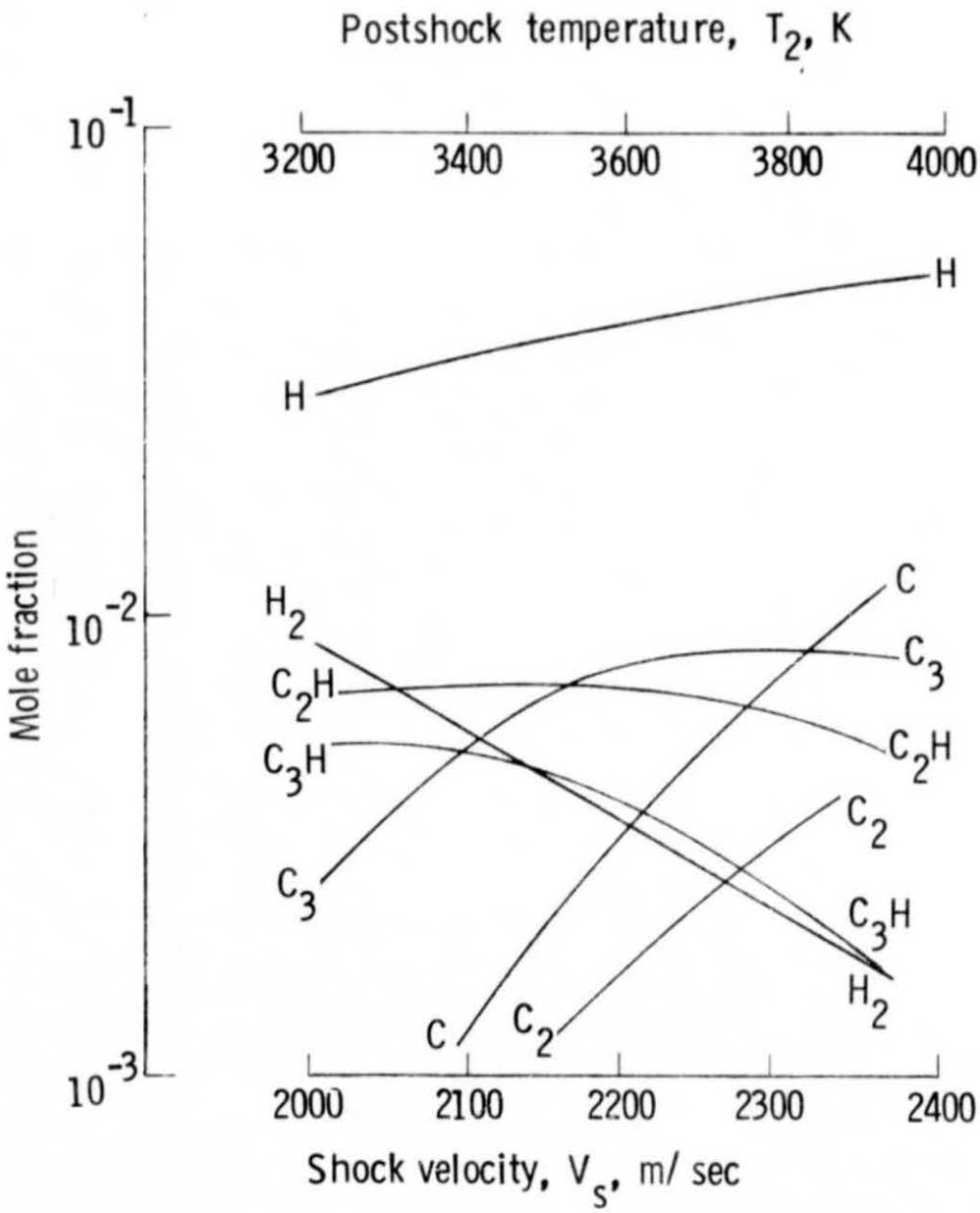

Figure 8. - Mole fractions of principal species behind a shock wave into a gas mixture of 97% argon, 3% C_2H_2. p_1 = 1.72 kN/m^2. (argon not shown)

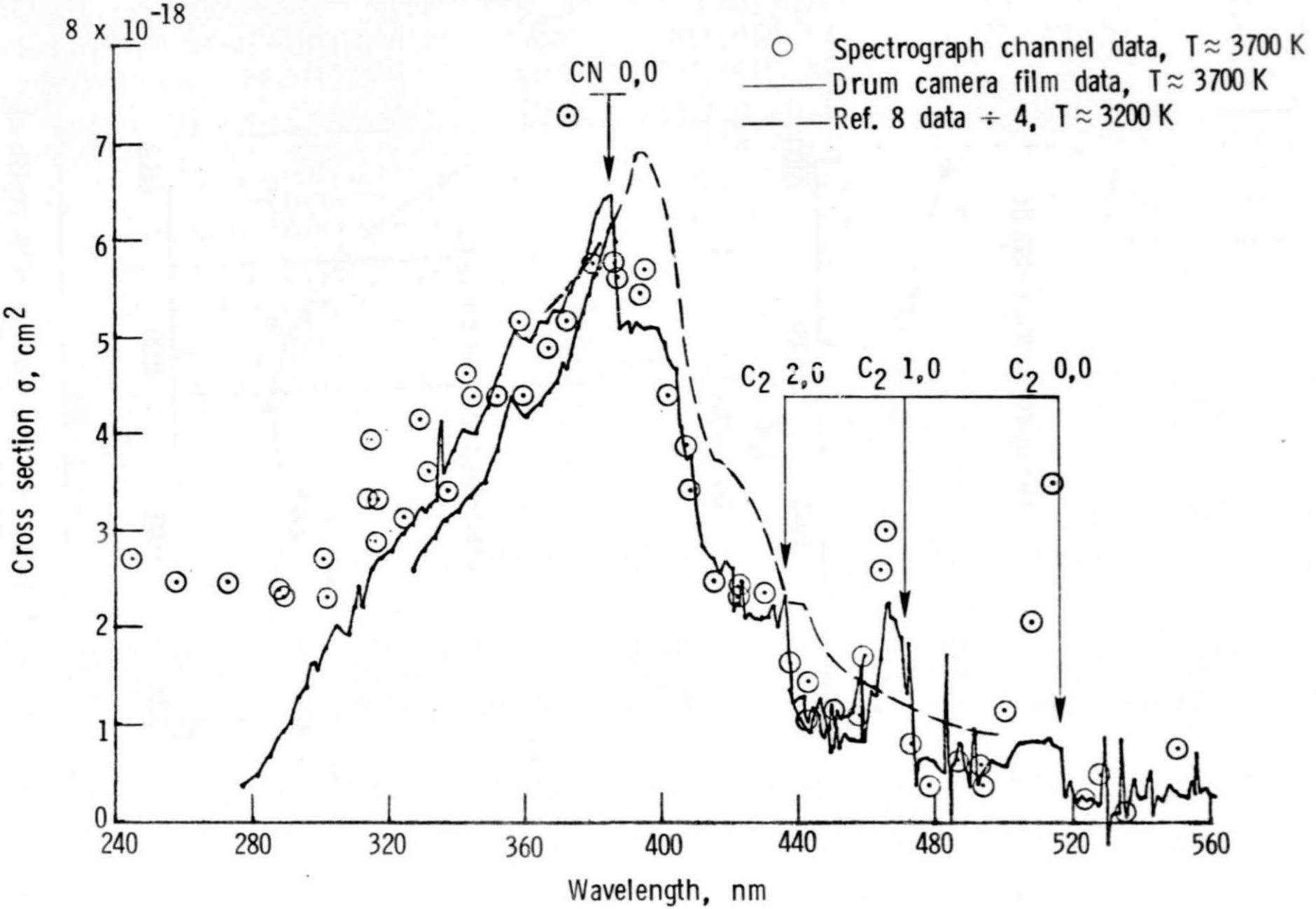

Figure 9. - Comparison of present cross-section measurement at T ≈ 3700 K with reference 8 data at T ≈ 3200 K.

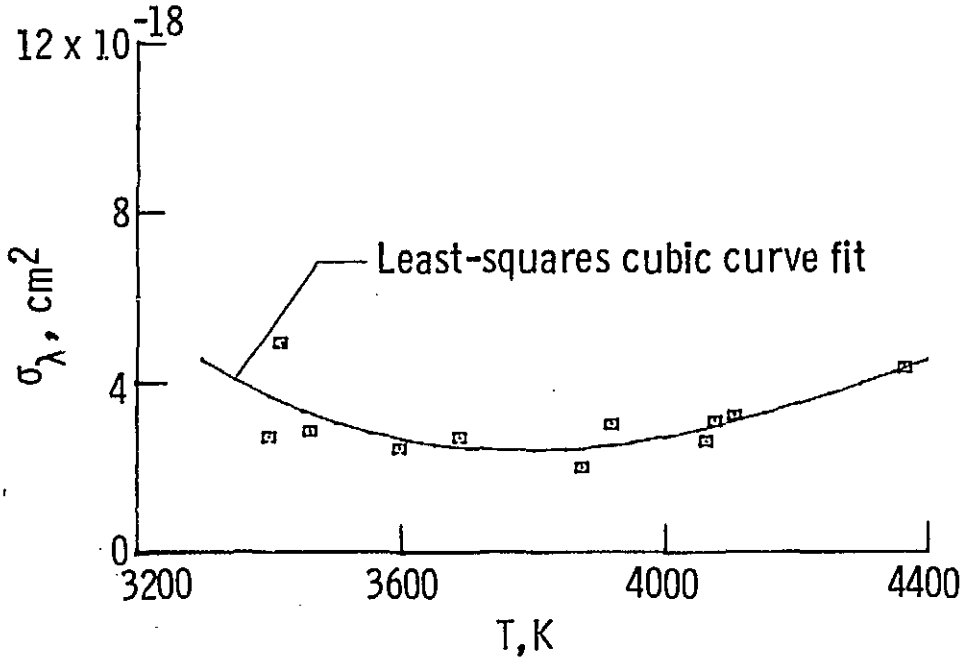

(a) λ = 310.

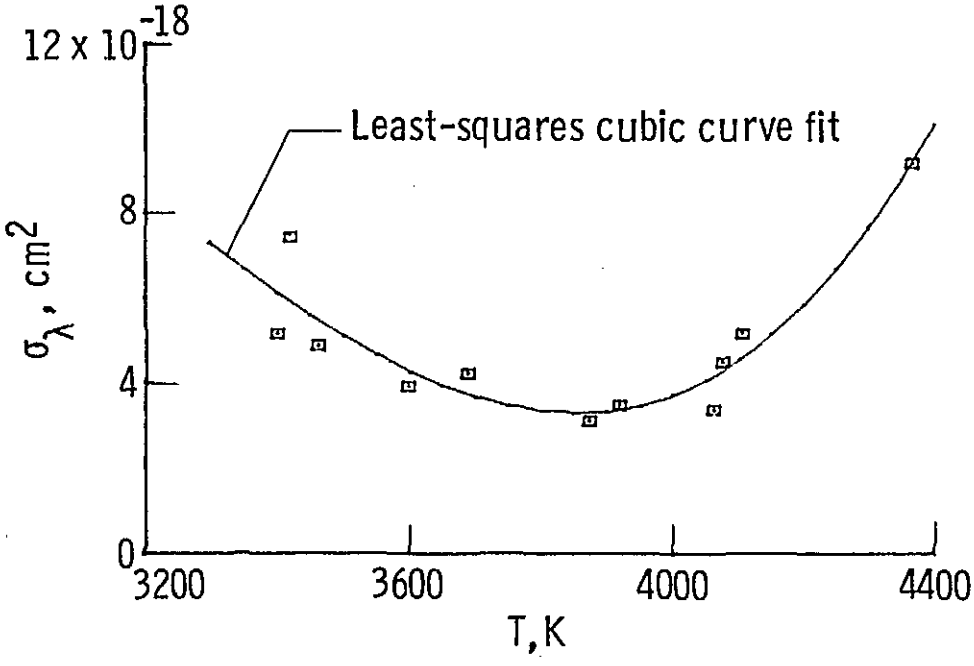

(b) λ = 344.

Figure 10. - Variation of absorption cross section with postshock temperature for selected wavelengths.

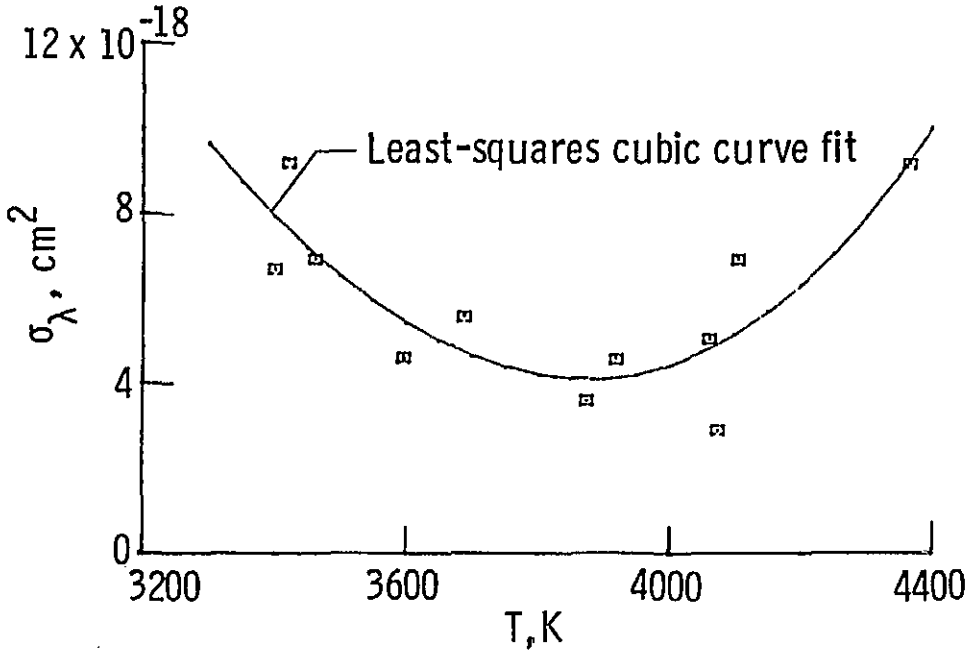

(c) λ=371.

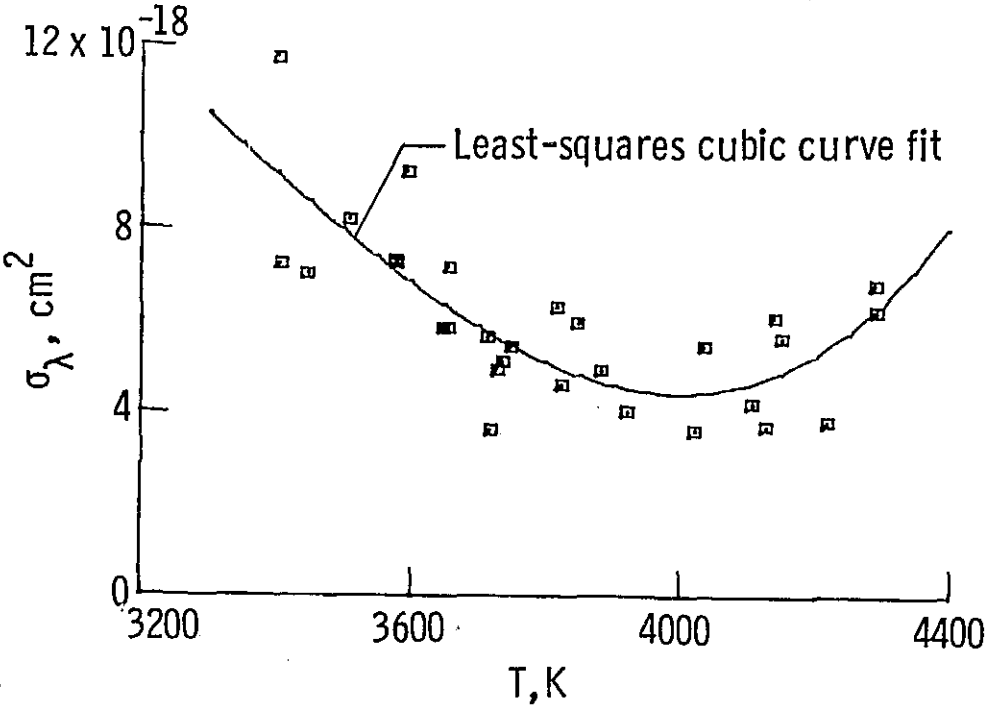

(d) λ = 405.

Figure 10. - Continued.

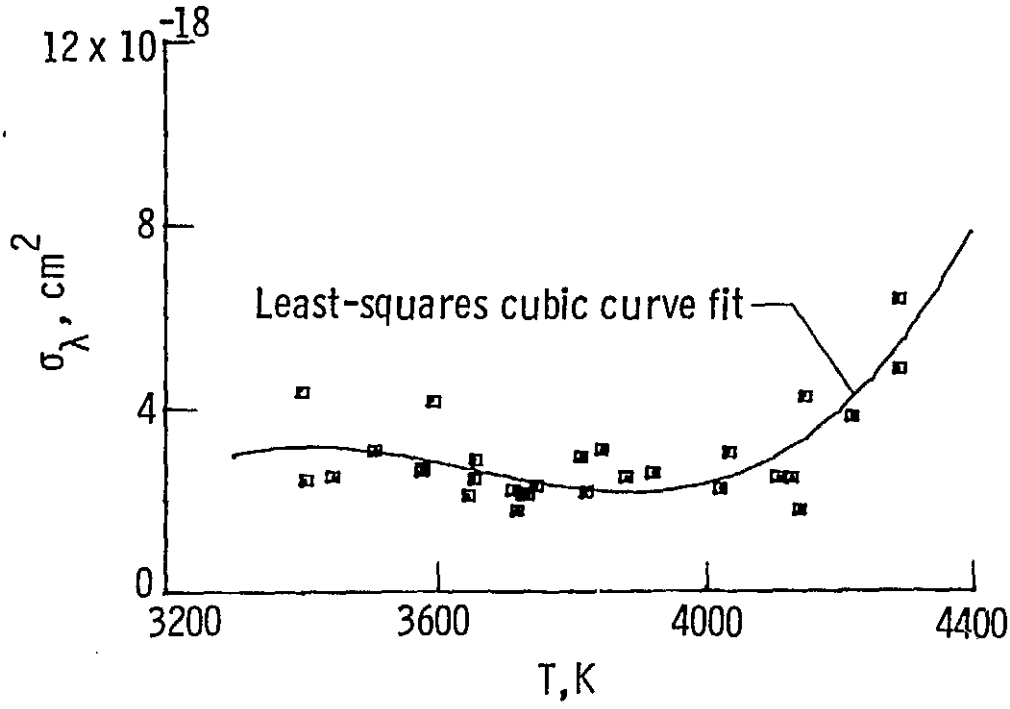

(e) λ = 434.

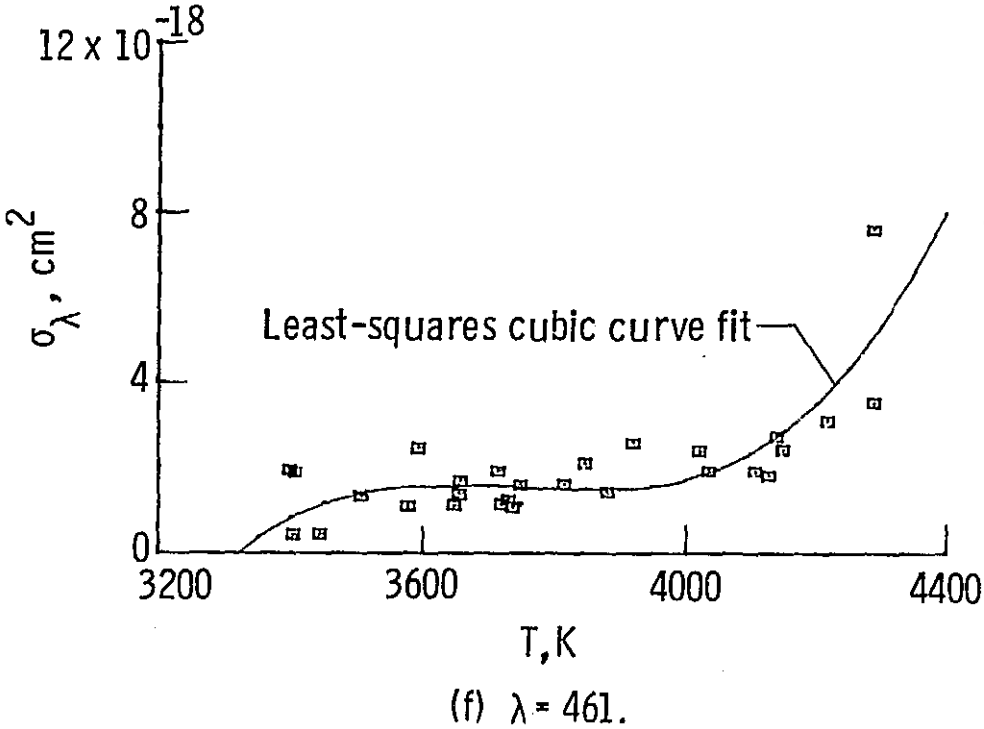

(f) λ = 461.

Figure 10. - Continued.

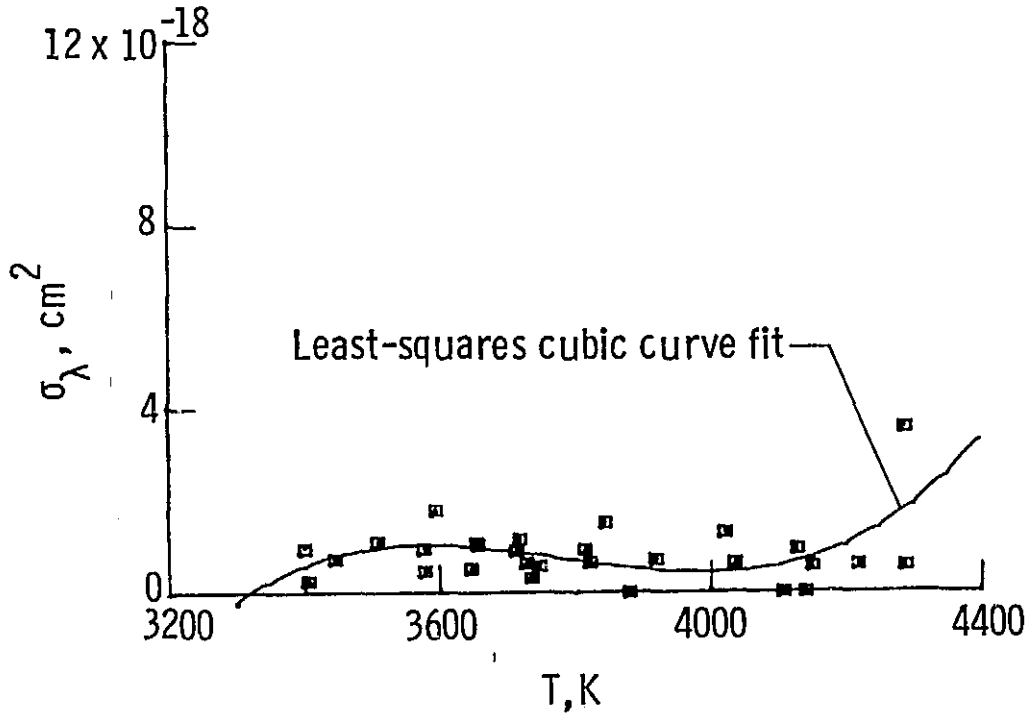

(g) λ = 490.

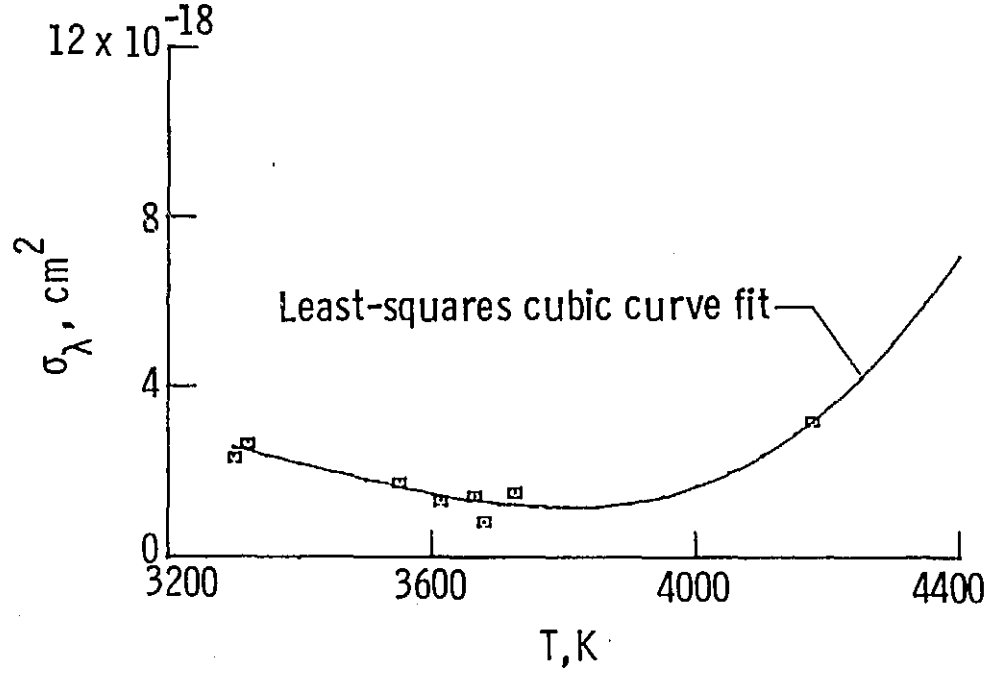

(h) λ = 537.

Figure 10. - Concluded.

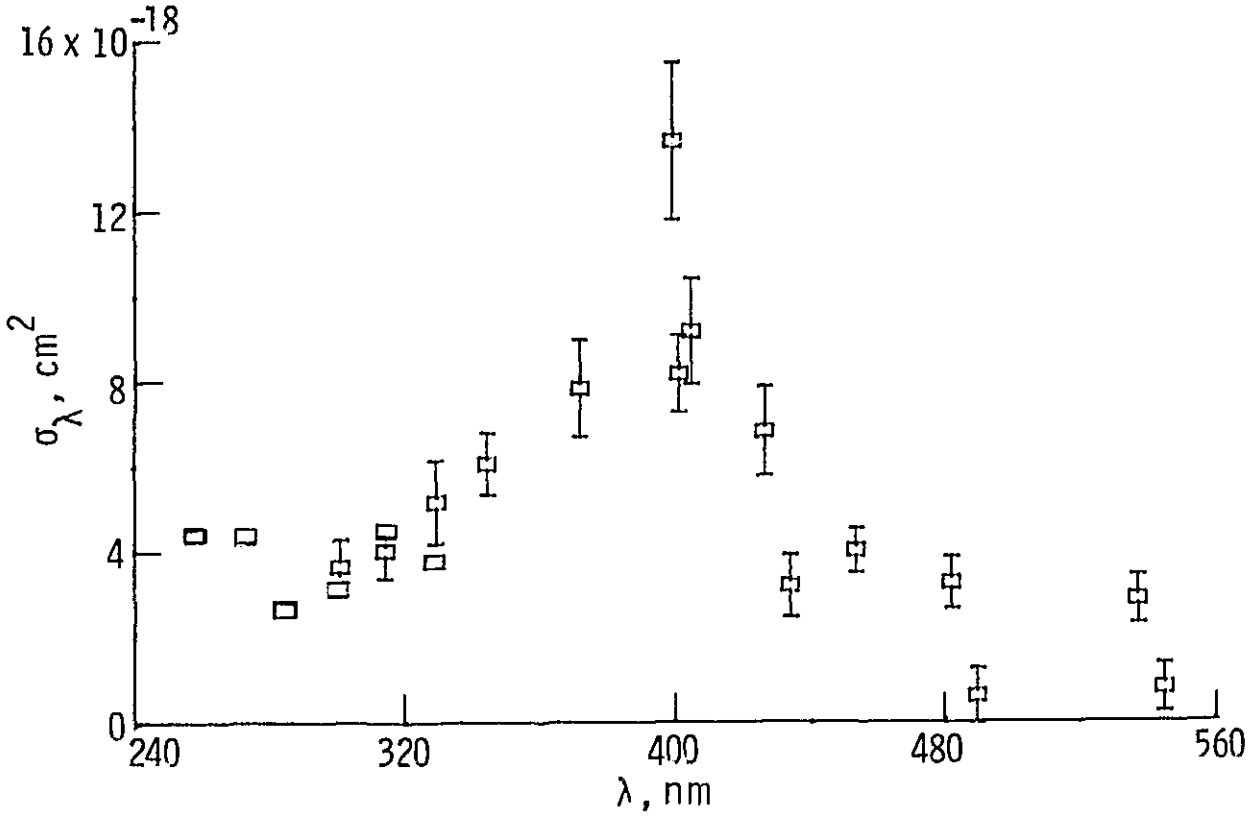

(a) T= 3400 K.

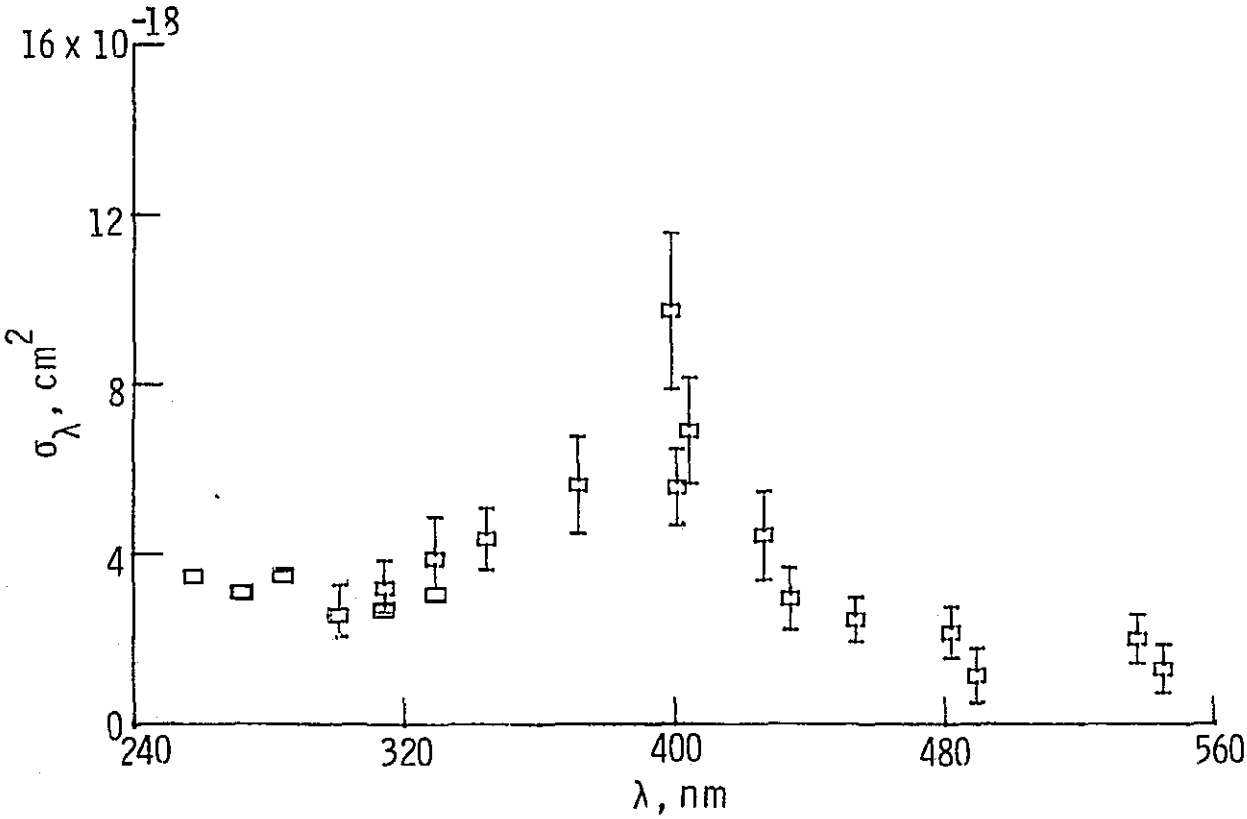

(b) T= 3600 K.

Figure 11. - Spectral cross-section profile at selected temperatures.
Symbol is value of cubic fit; bars indicate standard deviation of data.

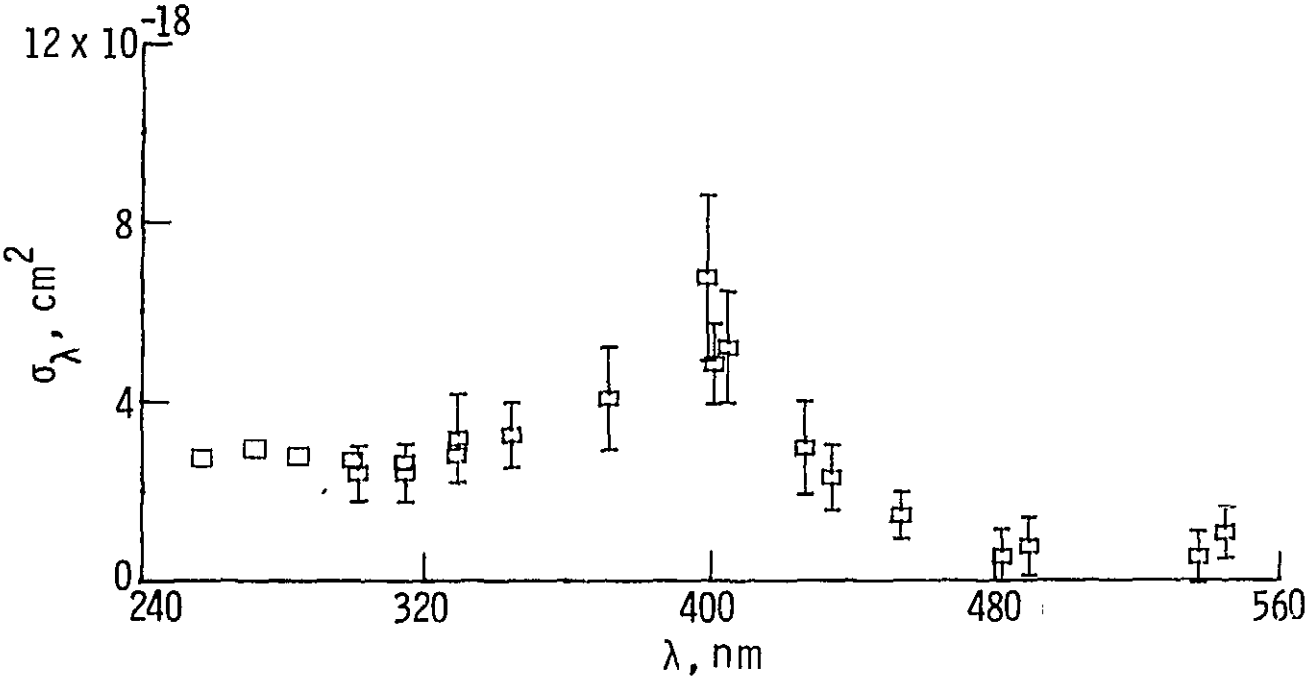

(c) T=3800 K.

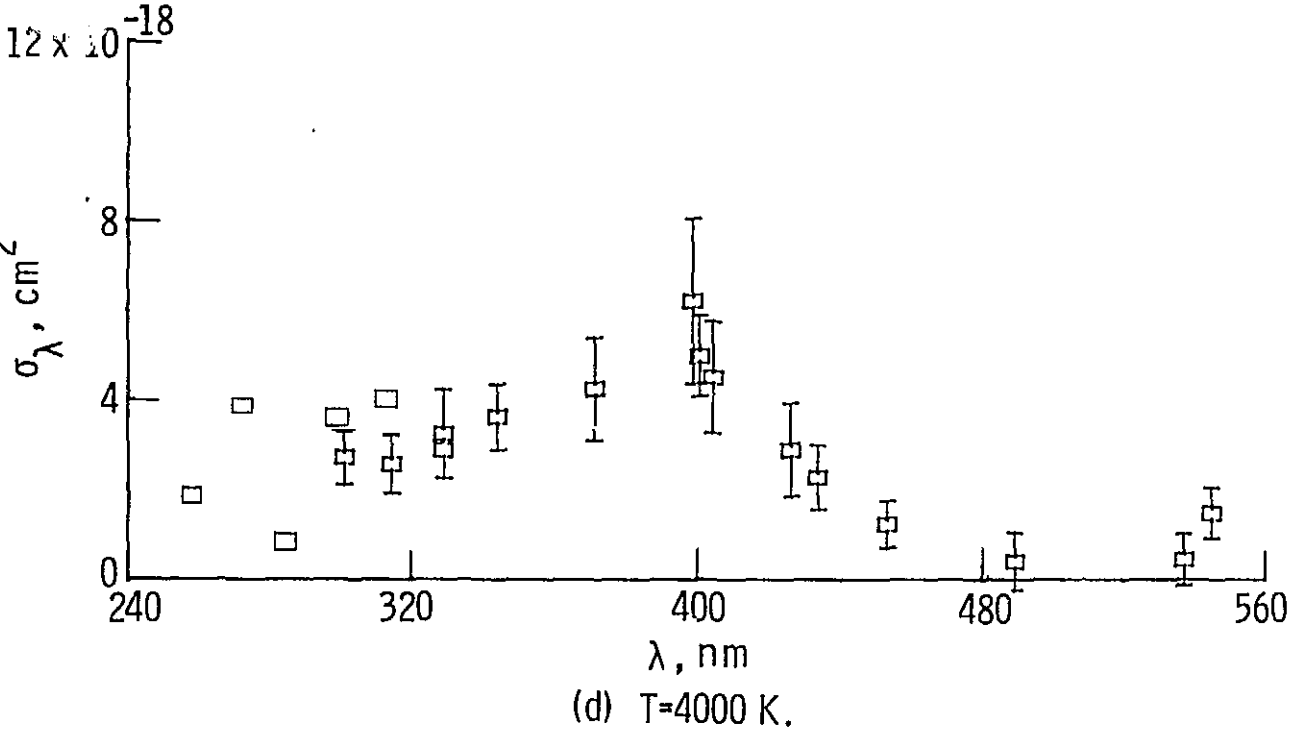

(d) T=4000 K.

Figure 11. - Concluded.

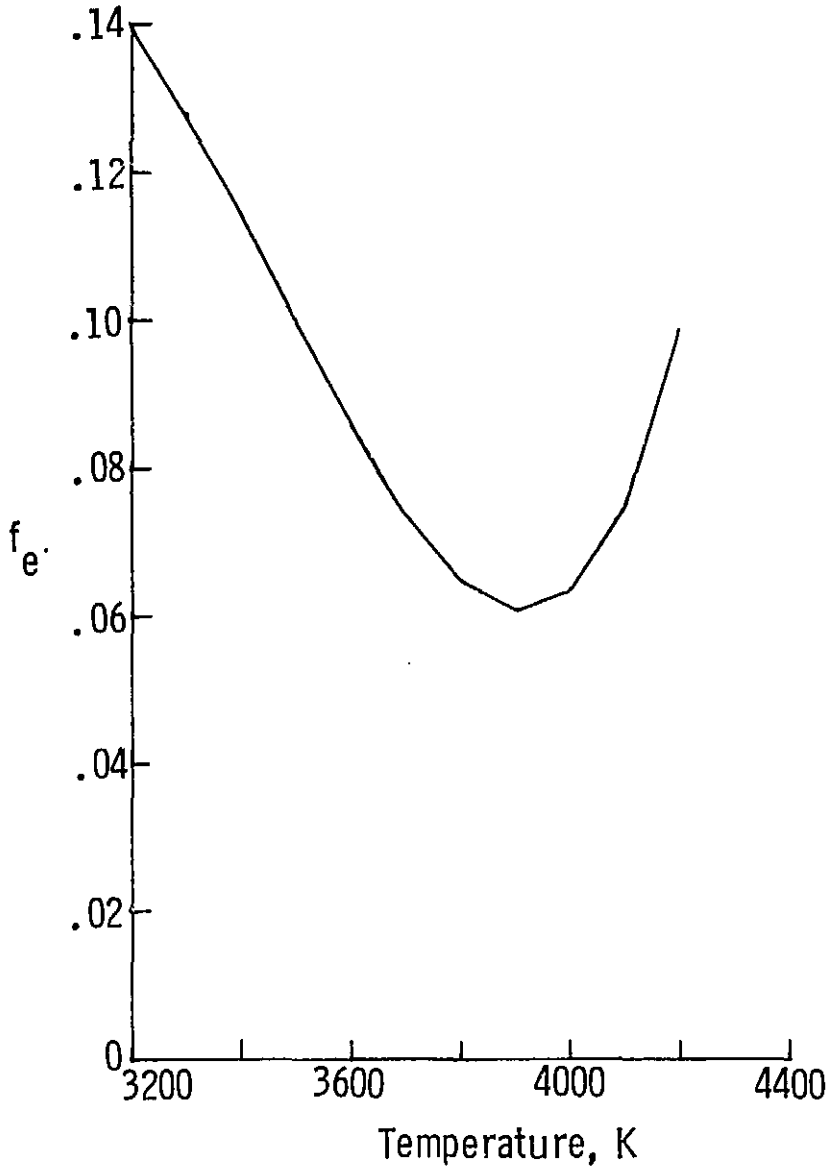

Figure 12. - Electronic oscillator strength calculated from present experiment as a function of test gas temperature.